UNIVERSITY OF CALIFORNIA
SANTA CRUZ

FUNCTIONAL, ANATOMICAL, AND GENETIC CHARACTERIZATION OF MOUSE RETINAL GANGLION CELLS

A dissertation submitted in partial satisfaction
of the requirements for the degree of

DOCTOR OF PHILOSOPHY

in

MOLECULAR, CELL AND DEVELOPMENTAL BIOLOGY

by

Erin Zampaglione

June 2016

The Dissertation of Erin Zampaglione
is approved:

Professor Alexander Sher (chair)

Professor David Feldheim

Professor Yi Zuo

Tyrus Miller
Vice Provost and Dean of Graduate Studies

TABLE OF CONTENTS

LIST OF FIGURES

ABSTRACT

Functional, Anatomical, and Genetic Characterization

Of Mouse Retinal Ganglion Cells

Erin Zampaglione

The retina is a remarkable piece of neural tissue, providing the gateway through which all visual information enters the mammalian nervous system. It is complex and highly organized, yet far more accessible to characterization than the brain. Furthermore, with its easy-to-manipulate input (images projected onto the retina) and well-defined output (neural code of the optic nerve), the retina lends itself beautifully to studying one of the fundamental questions of neuroscience: how do neurons encode information?

The retina is a multi-layered structure with intricate neural circuitry. In the outer layer are photoreceptors that translate light information into electrical signals, which are passed through a series of interneurons residing in the middle layer, and finally to the retinal ganglion cells (RGCs) in the inner layer. It is the RGCs whose axons form the optic nerve. Rather than simply relaying the raw light intensity values from the photoreceptors, the RGCs actually perform a wide variety of computational transformations to the signal, resulting in over 20 streams of parallel information being sent to the brain. These different types of RGCs can be classified using their distinct morphological features, expression of molecular markers, or electrophysiological functions. There is strong evidence that the morphology and gene expression of RGCs directly relate to their physiological response properties.

However, until we have an RGC classification scheme that incorporates these three aspects of neurons, we cannot fully understand how the retina develops, nor can we effectively explore the changes in the retina if it is damaged through disease or mutation.

In this thesis, I make progress in three major avenues that contribute to the understanding of mouse RGCs. One of the key methods I use is the characterization of physiological properties of RGCs using a large-scale multi-electrode array (MEA) recording system. In the first section, I describe my work that improves our ability to functionally characterize mouse RGCs. One project involves the development of a meta-analysis that compares white noise RGC responses across retinas showing we can consistently track 5 cell types across preparations. The second project describes my work developing an analysis pipeline for Direction Selective RGCs and improving the characterization of these well-studied subclasses. In the second section, I develop a technique to link the functional RGC with the morphological RGC on the MEA, using channelrhodopsin stimulation to link anatomical information to the cell's spiking information. In the third section, I used MEA recordings and my new analyses to determine how specific genes contribute to retinal circuitry. In one case I show a loss of all Direction Selective RGCs in a cell adhesion molecule (DSCAM) knockout mouse model, and in another case I show a loss of only one subtype of Direction Selective RGC in a developmental transcription factor (Satb1/Satb2) double knockout mouse model.

ACKNOWLEDGEMENTS

Science is a highly collaborative process, and it is with pleasure that I thank all the people who helped made this thesis possible. I would first and foremost like to thank my thesis advisor, Alexander Sher, who provided guidance and a physicist's perspective to all the problems I've had to solve. David Feldheim and Yi Zuo, as members of my thesis committee, provided valuable input in shaping the path of my thesis. Our collaborator Alan Litke was always prepared to dig deep into data to get to the bottom of a mystery.

I'd like to thank Arash Ng, whose training was vital to my success and who provided much of the initial data I used to build my analyses. My labmates throughout the years, Corinne Beier and Richard Smith, deserve awards for sitting through all those long retina meetings. I have to thank Shinya Ito for all his help with MATLAB and the never-ending conversations on spike sorting, Sergei Kachiguin for keeping the magic smoke inside all the electronics, and our undergrad Sydney Weiser, who enjoyed her experience enough to join the lab!

Many thanks go across the pond to our collaborators from the University of Strathclyde. Keith Mathieson and Filippo Pisano worked closely with me on the optogenetics project. Additionally, Jennifer Roebber and Niall McAlinden did much of the preliminary work to get that project off the ground.

I'd like to thank the Feldheim lab for being a constant source of entertainment (and reagents), and in particular Neal Sweeney for his knowledge of RGC

transcription factor expression and collaboration with the Satb1/2 project, and Jena Yamada for making sure everything always runs smoothly.

I would finally like to thank my parents and siblings whose good natured teasing was never unwelcome, my boyfriend John Forbes who supported me through everything, and all my friends scattered around the world for helping to keep my spirits high!

Several sections of this thesis contain work from manuscripts that are in preparation for publication. Chapter 3.2 (Matching Functional Cells with Anatomical Cells) is adapted from a first-author manuscript in preparation for submission to peer review. Chapter 3.3.1 (DSCAM Analysis) is adapted from a section of a second-author manuscript in preparation for submission to peer review. This section details only my contribution to the paper, which consists of the functional analysis of DS RGCs.

CHAPTER 1: INTRODUCTION

In this chapter I give context for my work within the field of neuroscience, provide background on the particular model and experimental paradigm I use, and present the motivation for my projects.

1.1 Study of Neural Systems

The study of neural systems is an exciting and rapidly growing field. So many fundamental aspects of human life – sensation, perception, behavior, and cognition – all stem directly from neuronal networks connected together in highly complex and precisely organized ways (Koch, 2004). Studying these circuits and their development gives insight into how their complexity arises, and how their organization contributes to function. A particularly important neural system is vision, which is responsible for a diverse range of tasks, such as perceiving shape, color, and motion, facilitating object and face recognition, and even synchronizing circadian rhythms (Kandel et al., 2000). How the brain takes the photons in its surrounding environment and processes them into the "mental picture" associated with visual perception is far from a straightforward task (Shimojo et al., 2001). For example, when a moving object creates a projection in the eye, that information proceeds into the brain via a variety of locations and pathways, splitting broadly into the dorsal stream that encodes its speed and location, and ventral stream that encodes its color, size, and form (Fig 1.1).

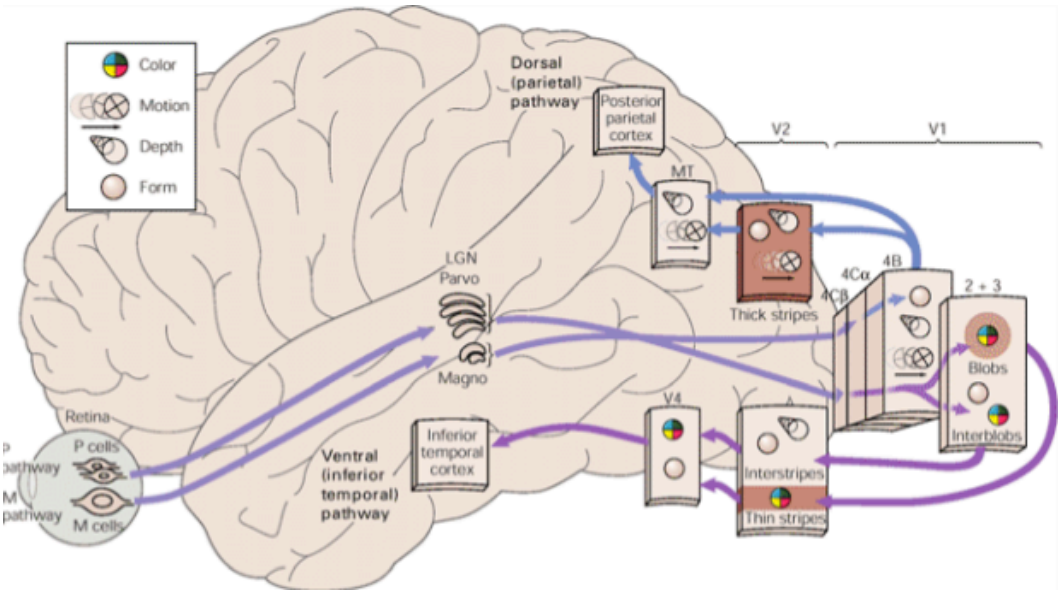

Figure 1.1: A brief overview of the organization of the visual pathway. Note the start of the pathway in the eyes, and how the information streams are split early on and processed in discrete locations throughout the brain. Adapted from (Kandel et al., 2000).

The neuron is the fundamental unit of a neural system, as it is the role of neurons to encode information. Neurons receive inputs, either by direct sensory information or by receiving the synaptic input from other neurons. Neurons then produce outputs called action potentials that initiate when there is a change in membrane voltage. Consider an example of the circuitry of a simple neural code (Fig 1.2). The output neuron can receive inhibitory inputs from neuron 1, and excitatory inputs from neurons 2 and 3 (Fig. 1.2A). The voltage trace of the output neuron shows that the cell would produce an action potential when it receives an input from ONLY neurons 2 and 3 (Fig. 1.2B). Thus, that output neuron integrates the information from the previous neurons and responds only when certain conditions are met.

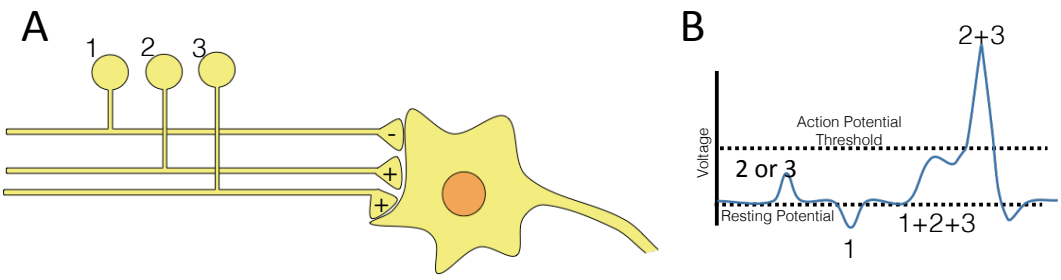

Figure 1.2: A simple neural code. A) Shows three neuronal axons synapsing onto the dendrites of a fourth neuron. Two of the input neurons are excitatory, and one is inhibitory. B) A graph of the membrane potential reading of the output neuron. A single input from 2 or 3 does not meet the action potential threshold. The input from 1, 2 and 3 also cannot induce an action potential. Thus, this output neuron is coded to only spike in a specific circumstance, that is, when it receives input from neurons 2 and 3, but not 1. Adapted from (Kandel et al., 2000).

1.2 Organization of the Retina

My research focuses on the retina, the first step in the visual pathway. Although the retina is a sensory organ, it actually develops from the central nervous system, rather than the peripheral nervous system. Because of this, the retina shares many structural and molecular similarities to the brain, and can be used as a model for studying certain aspects of cortical features such as its laminar organization, response to injury, and specialized immune responses (London et al., 2013). When light passes through the front of the eye, the cornea, lens and pupil focus the rays so that the image appears inverted on the retinal surface (Fig. 1.3A). The retina itself is a thin piece of neural tissue that lines the back of the eye (Fig 1.3B).

Far from a simple photon detector, the retina is highly organized, with a distinct layered structure and over 50 types of cells that can be divided into five main groups: the photoreceptors, horizontal cells, bipolar cells, amacrine cells, and retinal

ganglion cells (Masland, 2001). Photons that hit the retina are detected by rod and cone photoreceptors in the Outer Nuclear Layer (ONL) and converted into an electrical signal via a G-protein coupled receptor signal transduction pathway (Ebrey and Koutalos, 2001). In the Outer Plexiform Layer (OPL), photoreceptors synapse onto the dendrites of bipolar cells. At this synapse, there is lateral integration and feedback to photoreceptors that comes from the very broad-reaching dendrites of horizontal cells (Thoreson et al., 2008). The cell bodies, or somas, of bipolar cells comprise the Inner Nuclear Layer (INL). There are at least 13 known types of bipolar cells, broadly grouped into ON bipolar cells, which respond when the cones detect light, OFF bipolar cells, which respond when the cones do not detect light, and rod bipolar cells, which respond when rods detect light (Euler et al., 2014). Their axons terminate in the Inner Plexiform Layer (IPL), with OFF bipolar cells stratifying in the upper portion of the IPL, and ON bipolar cells stratifying in the lower portion of the IPL. Multiple bipolar cell axons then synapse onto the retinal ganglion cells (RGCs), whose cell bodies reside in the Ganglion Cell Layer (GCL), and whose axons comprise the optic nerve. At the INL synapse there are over 30 types of amacrine cells that mediate lateral integrations and functional inputs to the RGC layer (Rodieck, 1998).

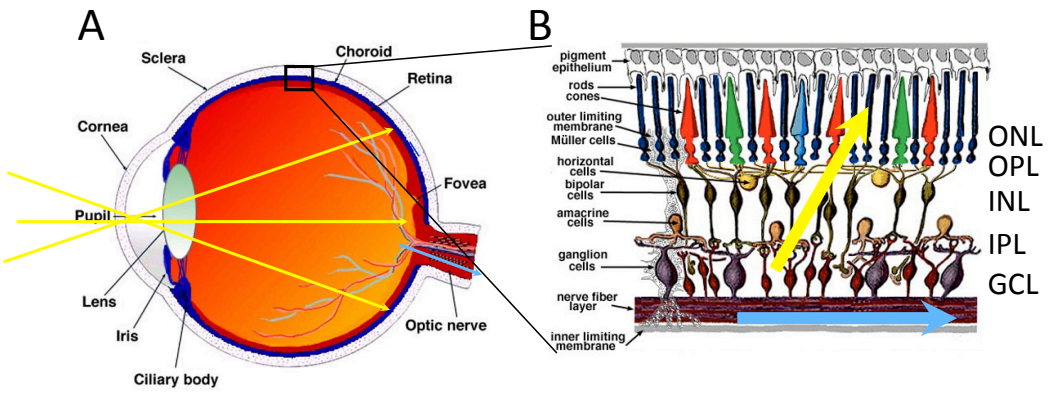

Figure 1.3: Schematic of the eye and retina. A) Cross section of a mammalian (human) eyeball, showing the retina lining the back of the eye. B) Expanded section of the retina neuronal circuits. Note the orientation of the layered structure, with the photoreceptors furthest from the light and the RGCs sitting in front of them. Yellow arrows indicate light path, blue arrows indicate flow of information to the brain. Adapted from http://webvision.med.utah.edu/

1.3 Parallel Processing in the Retina

Importantly, even at the very first photoreceptor-to-bipolar synapse, there is a split in the flow of information, resulting in what is termed "parallel processing" (for review, see (Wässle, 2004)). This results in over twenty parallel streams of information being sent to the brain, each from a different type of RGC that encodes a specific feature of the visual scene such as the onset or offset of light, motion, or color (Rodieck, 1998).

These various types of RGCs have differences in anatomical form that directly contribute to differences in function. For example, an RGC with a broader dendritic field will contact more bipolar cells and thus have a larger field of view, or the dendrites of an RGC will laminate such that they specifically contact ON or OFF bipolar cells to determine its ON or OFF properties (Fig 1.4A). The wide variety of RGCs, in terms of their anatomical diversity as well as their specific wiring to the

different bipolar and amacrine cells, makes them interesting from a developmental perspective (what transcription factors and signals are required to create each unique population?) as well as from a neural coding perspective (how do these different filters provide relevant information to the brain?).

As any one RGC only contacts a subset of bipolar cells, there is a phenomenon of "mosaic tiling", in which the dendritic fields of all RGCs of a single type cover the retinal area without overlapping (Wassle et al., 1981; Dacey, 1993). As a consequence, the "receptive fields", or area of sensitivity, of those RGCs tile the visual space (Devries and Baylor, 1997; Field and Chichilnisky, 2007; Petrusca et al., 2007; Gauthier et al., 2009; Anishchenko et al., 2010; Sher and DeVries, 2012), sampling the whole visual field for the feature they detect (Fig 1.4B). Again emphasizing the parallel nature of this information pipeline, the mouse RGCs come together in the optic nerve, but ultimately project to approximately 46 different brain targets, including the lateral geniculate nucleus, olivary pretectal nucleus, suprachiasmic nucleus, and the amygdala. (Morin and Studholme, 2014).

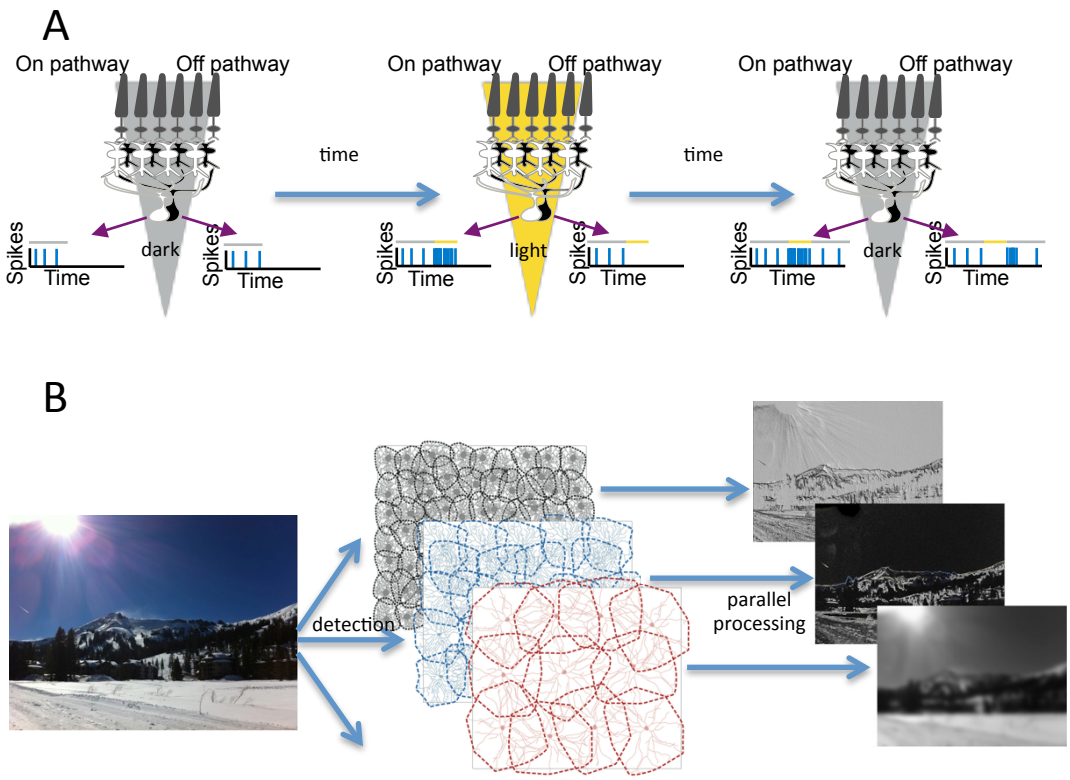

Figure 1.4: Examples of the retinal parallel pathway. A) Simple illustration of the ON and OFF pathways. A stimulus goes from dark to light to dark again as a function of time. Although the two RGCs are exposed to the same light, their spike trains are different because of their differential wiring to the ON vs OFF bipolar cells. B) More complex parallel pathways, showing a several different RGC populations that sample the same section of the visual field, but extract different information, such as motion (top right image), edges (center right) or luminance (bottom right). Adapted from (Dhande et al, 2015).

1.4 Retinal Ganglion Cells

Thus the focus of my work narrows to the realm of RGCs, the output cells of the retina and final stage of the retinal parallel processing pathway. In particular, my work utilizes the mouse retina and mouse RGCs. Although much of historical vision research has been done on monkey, cat, rabbit, rat, and guinea pig, our research

focuses on mouse models for a number of reasons. The major draw of mouse studies is their small size, relatively simple maintenance, and the availability of genetic mutants and other genetic manipulation tools such as the Cre-loxP system to turn on fluorescent reporters or delete genes of interest, and transgenically introduced GFP expression to either randomly or non-randomly label subgroups of RGC. In addition, mice boast a sophisticated visual system, both in the retina and in the higher brain structures, that can provide reasonable insight to other, more complicated mammalian visual systems (Huberman and Niell, 2011).

There are approximately 30 known types of RGCs, which have been characterized through their functional responses (Van Wyk et al., 2009; Badea and Nathans, 2011; Farrow and Masland, 2011), anatomical features (Sun et al., 2002; Coombs et al., 2006; Völgyi et al., 2009), and molecular expressions (Xiang et al., 1995; Huberman et al., 2008, 2009; Rivlin-Etzion et al., 2011). Functional characterization (Fig 1.5A) focuses on the RGC response to visual stimulation, with classification focusing on properties such as ON versus OFF response, transient versus sustained response, and direction or orientation selectivity (Carcieri et al., 2003; Farrow and Masland, 2011; Baden et al., 2016). Anatomical classification (Fig 1.5B) has been done through dye filling and imaging, with classification focusing on features such as the size of the dendritic field, branching of the dendrites, and stratification patterns (Doi et al., 1995; Kong et al., 2005). Molecular characterization (Fig 1.5C) occurs through labeled mouse cell lines or discovered molecular markers

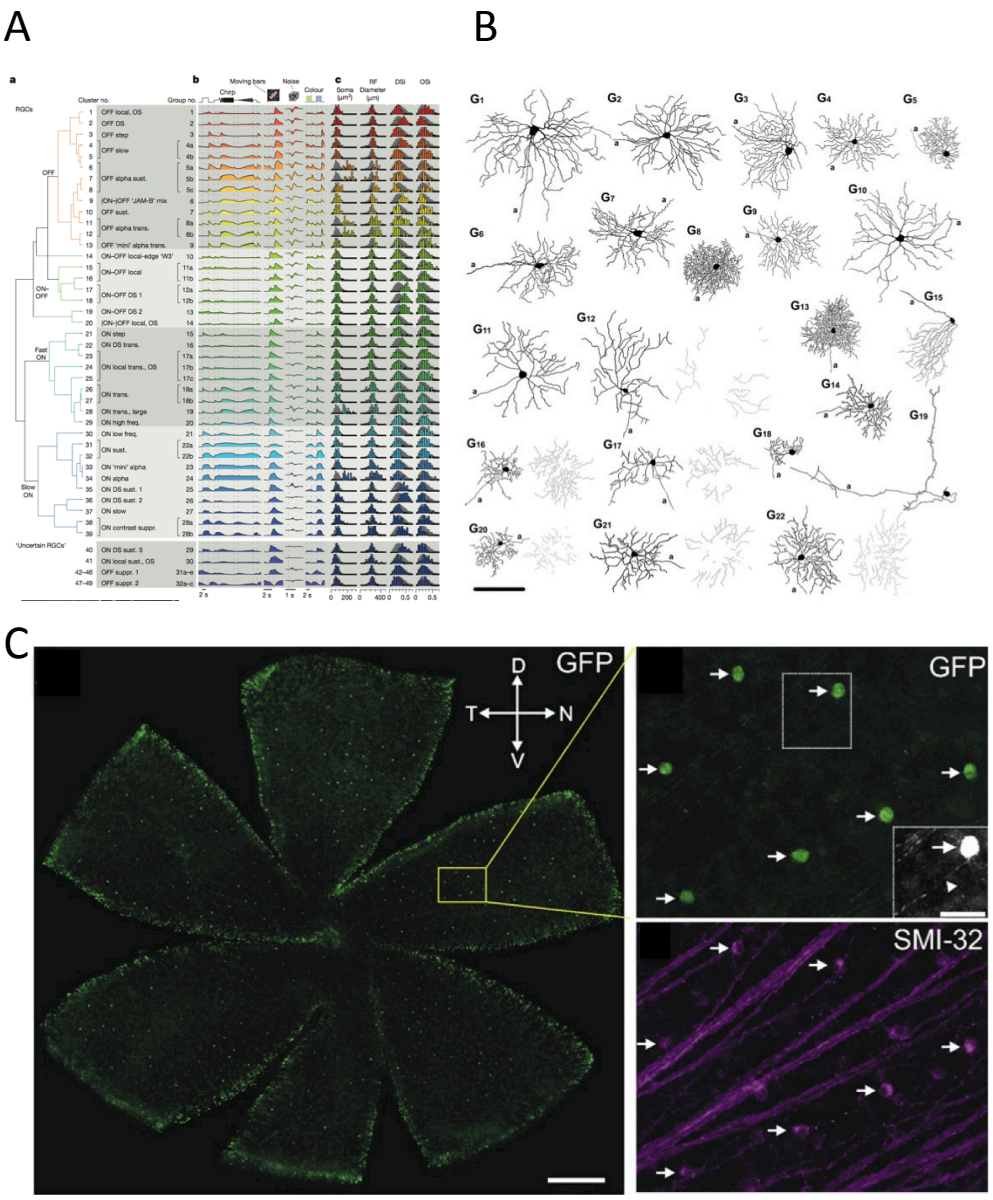

Figure 1.5: Functional, Anatomical, and Genetic identification strategies. A) Functional characterization of RGCs using a series of different visual stimuli. Adapted from (Baden et al, 2016). B) Anatomical characterization of RGCs showing a variety of dendritic sizes, branching, and stratification. Scale bar = 100µm. Adapted from (Volgyi et al, 2009). C) Expression pattern of CB2-GFP mice, which have a transgene such that GFP is expressed in a subset of RGCs with regular spacing, SMI-32 expression, and an OFF-transient light response. Left scale bar = 500 µm, right scale bar = 50 µm. Adapted from (Huberman et al, 2008).

that label a specific subset of RGCs (Huberman et al., 2008, 2009; Kay et al., 2011a), and is often verified by looking at function or anatomy, or the nonrandom mosaic tiling of the cell dendritic fields (Sümbül et al., 2014).

1.5 Functional Types of Retinal Ganglion Cells

While all three methods of RGC identification are important, it is ultimately their functional identity that is relevant to the downstream visual system – if an RGC can change some aspect of its shape or gene expression without affecting its output, the information pathway remains essentially unperturbed. Thus we will consider a brief overview of some already known cell types in terms of their broad functional classes, although many of these can be divided into subclasses (for review, see (Dhande et al., 2015; Sanes and Masland, 2015)).

The simplest known types of RGC are the local spot detectors, also known as "center/surround cells" or "alpha cells" (Kuffler, 1953; Boycott and Wässle, 1974). These respond either to the onset or offset of light with either a transient or sustained spike response (Pang et al., 2003; Van Wyk et al., 2009). Another group of simple-receptive field RGCs are local edge detectors, which detect small dark moving objects on a stationary background (Zhang et al., 2012).

Orientation Selective (OS) RGCs are a functional type with a more complicated receptive field, responding to stationary or moving bars that are oriented in a particular direction, and do not respond to bars oriented perpendicular to that

direction (Zhao et al., 2013; Nath and Schwartz, 2016). There are two main subtypes, which correspond to either the horizontal or vertical orientation.

There are several types of mouse RGCs that are considered Direction Selective (DS) that have been shown to respond to motion in a single direction, and be suppressed by motion in the opposite direction. These are broadly categorized into three types. First are ON/OFF DS RGCs (Oyster and Barlow, 1967; Oyster et al., 1972), of which there are four subtypes that correspond to the four cardinal directions. ON DS RGCs respond to slower speeds and are sensitive to motion in three directions (Oyster and Barlow, 1967; Oyster et al., 1972). Finally, there is one identified group of OFF DS RGCs, which respond to the offset of light and to motion in an upward direction (Kim et al., 2008).

Finally, there is a subset of RGCs known as intrinsically photosensitive RGCs (ipRGCs), which express an opsin molecule called melanopsin (Provencio et al., 2000). These cells are connected to photoreceptors, but are also independently sensitive to light (Berson et al., 2002). There are currently five known subtypes, and are involved in maintaining circadian cycling, as well as encoding global ambient light levels and contrast information (Hattar et al., 2002; Schmidt et al., 2014; Zhao et al., 2014).

1.6 Micro-Electrode Array Recordings

In order to study the neural code of the RGCs, the spike patterns need to be observed, recorded, and correlated to visual inputs. There are many techniques

available for recording neuronal action potentials, each with unique advantages and shortcomings. Patch clamp is a technique that can record intracellularly from a single cell, and single unit electrodes can record extracellular from one or two cells, both giving high temporal resolution for the cell's voltage changes. However, these are low-throughput techniques that are very laborious, and can record from a limited number of cells per preparation (Schmidt and Kofuji, 2011). On the other end of the spectrum, calcium dye imaging can record from many cells simultaneously, but does not have the ability to resolve individual spikes (Baden et al., 2016).

The multi-electrode array (MEA) recording (Fig 1.6A,B) allows us to detect action potentials generated by hundreds of RGCs in a single preparation. In particular, we use a custom built high density MEA that was designed and built at the University of California Santa Cruz by the Santa Cruz Institute of Particle Physics (SCIPP) (Litke et al., 2004). In this technique, a flat slice of neural tissue is placed over a planar array of 512 electrodes with either 30μm or 60μm spacing. The tissue is perfused with an oxygenated nutrient medium, and extracellular voltages are recorded at 20 kHz and stored offline to be processed into spike timing information (see Methods). In the case of studying RGCs, a small, intact piece of retina is carefully removed from the back of an enucleated eye and placed RGC side down on the electrode array. An optically reduced CRT image is displayed to the photoreceptors, and because the vertical synaptic pathway remains intact, the retina responds in a similar fashion to the in-vivo situation, with photoreceptor responses being transformed through interneurons and the signal then passing to the RGC layer. Using

this method allows us to record high-resolution spike timing information from hundreds of RGCs simultaneously. However, one major disadvantage to the MEA system is that it is not readily apparent which anatomical neuron gave rise to a particular spike train. The reasons for this are that the extracellular recording allows for only approximate locating of the cell body, and the density of RGCs cell bodies is such that it remains ambiguous.

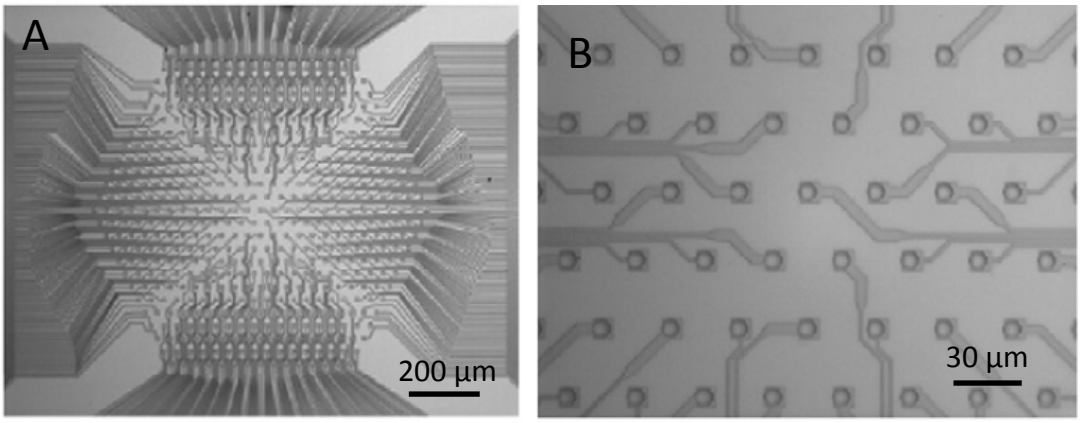

Figure 1.6: Images of the MEA surface. A) The full 30 µm array has 519 electrodes arranged in a hexagonal pattern with 450 µm sides, with all traces extending outward. B) A close up shows the electrodes in the center of the array. (Adapted from Gunning et. al, 2007)

1.7 Overarching Motivation

The ability to better identify and understand RGC types will be incredibly useful for many future analyses. The three main branches of this thesis show clear advances in all aspects of RGC characterization. I begin with improvements in functional characterization of RGCs in the MEA paradigm, where my unique opportunities for high-density, high throughput recording allow me to analyze many cells with many stimuli in novel ways. My analyses that are able to classify white

noise responses across preparations and DS responses in great detail provide a framework for understanding the functional properties of RGCs. I then move on to addressing the major disadvantage of the MEA system, developing a technique that matches functional spike trains to anatomical cells using an optogenetics-based approach. Finally, I tackle the ultimate goals of these techniques by using some of the analyses I developed to compare wildtype retinal responses to mutant retinal responses, providing insight into the contributions of several genes on RGC function.

With this information, any lab interested in retinal circuitry will have more freedom to examine mutations that produce subtle effects on RGC development or function. These effects may have downstream consequences in visual cortex, which can be studied with fMRI and single unit recordings, or produce behavioral changes, which can be studied using psychophysics. Thus my work contributes to the understanding of retinal development, the visual system, and possibly origins of genetic visual deficits.

CHAPTER 2: METHODS

In this chapter I have aggregated the experimental and analytical protocols I used throughout my thesis. As many of these methods were used in multiple projects, it is convenient to group them here.

2.1 Mice

Animals were cared for and used in accordance with guidelines of the U.S. Public Health Service Policy on Humane Care and Use of Laboratory Animals and the NIH Guide for the Care and Use of Laboratory Animals. All procedures were performed in accordance with the UCSC Institutional Animal Care and Use Committee. All mice were purchased from Jackson Laboratories, and were backcrossed to C57Bl/6 lines in the laboratory.

Genotyping was done using DNA from a tail clip. Initial testing of the ChR project was done on Thy1-ChR-YFP strains (JAX 007615). These mice were identified as positive for the transgene with primers against GFP (5'-CCTA CGGCGTGCAGTGCTTCAGC-3' and 5'-CGGCGAGCTGCACGCTGCGTCCTC-3'). Cre lines used included CRH-ires-Cre (JAX 012704) and Grik4-Cre (JAX 006474). These mice were identified as positive for their transgenes with primers against CRH-ires-Cre (5'-CAATGTATCTTATCATGTCTGGATCC-3' and 5'-CTTACACATTTCGTCCTAGCC-3') or a general Cre primer (5'-ACCAGA GACGGAAATCCATCG-3' and 5'-TGCCACGACCAAGTGACAGCAATG-3'). Cre lines were crossed to a Rosa26-fsf-chR-tdTom (JAX 01256) strain. Mice were

identified as positive for this transgene with primers against ChR-tdTom (5'-CTGTTCCTGTACGGCATG G-3' and 5'-GGCATTAAAGCAGCGTATCC-3'). For the mutant analyses, Dr. Peter Fuerest in the Fuerest lab (Department of Biological Sciences, University of Idaho) provided DSCAM mutant mice, and Satb1/2 mutant mice were provided by Dr. Neal Sweeney and Dr. David Feldheim in the Feldheim lab (MCD Biology, UC Santa Cruz).

2.2 Data Acquisition

Mice were dark adapted for 20-30 minutes, then anesthetized with ~0.4mL of a cocktail of 16mg/mL ketamine and 4mg/mL xylazine in PBS. Following cervical dislocation, one eye was enucleated under dim red light. The anterior of the eye and vitreous were removed and an approximately 1mm^2 piece of retina was isolated from the sclera. The piece was placed RGC side down over the planar MEA while being perfused with oxygenated, bicarbonate buffered Ames' solution kept at 32.4°C. The relative location of the piece in relation to retinal coordinates was determined using the vasculature in the eyecup (Wei et al., 2010), and orientation of the piece on the array was determined using axon track direction from the recording.

Two arrays were used over the course of my thesis. One was a 512 electrode MEA with 30µm spacing, and covering a rectangular area of 1.7mm^2. The other had 519 electrodes (although 7 were dead so as to match the 512 acquisition system) that were arranged in a hexagonal shape 450µm on each side, covering an area approximately 0.526mm^2. The electrodes were spaced 30µm apart in a triangular grid

(Gunning et al., 2007). As described previously, (Litke et al., 2004) voltages from the electrodes were digitized at 20 kHz and stored offline for further processing.

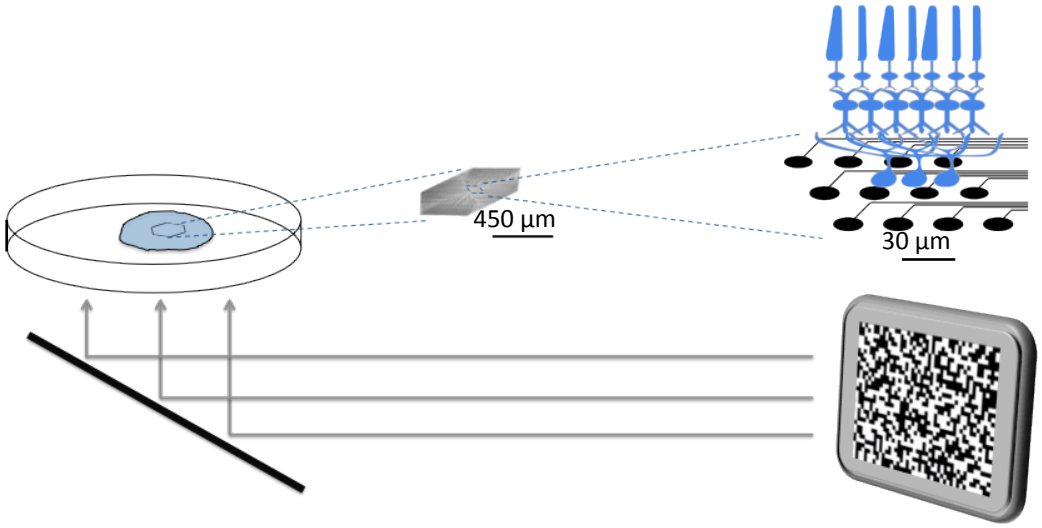

Figure 2.1: MEA recording setup schematic. Stimulation begins as an image on a CRT monitor, and is optically reduced and projected onto the MEA. A small section of retina is placed RGC side down over the electrodes, such that the normal light response circuit remains intact. Extracellular voltages are recorded during stimulation and later processed into spiking information from the RGCs.

2.3 Visual Stimulation

Visual stimulation was generated using a custom LISP code (Chichilnisky, 2001) or a custom MATLAB code by Daniele Fusi, and displayed on a CRT monitor with a refresh rate of 120 Hz. The image was optically reduced onto the retina at a resolution of 9µm/pixel. Several types of visual stimulation were used throughout this thesis. Each different type of visual stimulation provides a different way to characterize RGCs and requires a different type of analysis. The visual stimuli will be described here so that their analyses can be described after.

The binary spatio-temporal white noise stimulus consists of a flickering black and white square grid, with each square following a Bernoulli distribution with p = 0.5, uncorrelated to the others in both space and time. The checkerboard had either 45x45 μm^2 squares with 60 Hz updating, or 90x90 μm^2 squares with 30 Hz updating (Fig 2.2A).

The single Direction Selective (DS) stimulus consisted of full field drifting square waves that were randomly presented in 16 different directions (Fig 2.2B). Each direction was presented 5 times, each time for a duration 10 seconds followed by 3 seconds of gray screen. The spatial period was 576μm, and the temporal period was 1.07 seconds. To put that in an in-vivo perspective (ie, considering the images as if they were displayed to a living mouse through their lens and cornea), the spatial frequency would be ~0.054 cycles/degree, and the drift frequency would be ~0.938 cycles/second (Remtulla and Hallett, 1985).

The DS parameter scan stimulus consisted of sinusoidal gratings in 8 equally spaced directions, 5 spatial periods evenly spaced on the logarithmic scale (144μm, 288μm, 576μm, 1152μm, 2304μm), and 5 temporal periods evenly spaced on the logarithmic scale (0.13 sec, 0.27 sec, 0.53 sec, 1.07 sec, 2.13 sec), for a total of 200 unique parameter combinations. These 200 parameter combinations were presented for 5 seconds each, with 2.5 seconds grey screen in between. The presentations were randomly shuffled within one trial, and 5 trials were used in each experiment (Fig 2.2C).

A final stimulus used was a full field flash, which consisted of the entire screen alternating black, grey, white, grey for 2-second intervals (8 seconds for a single cycle) and 150 trials (Fig 2.2D).

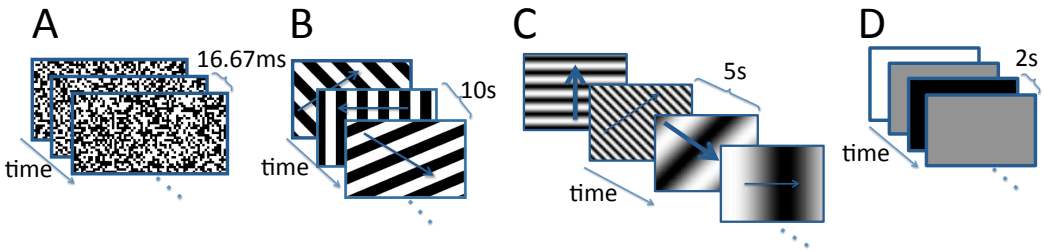

Figure 2.2: Schematic of the different stimuli used throughout experiments. A) Binary spatio-temporal white noise. B) Single parameter full field drifting square waves. C) Multiparameter full field drifting gratings. D) Full field flashes.

2.4 Data Processing Overview

The processing of electrophysiological data, consists of several steps. First, the voltages recorded are translated into individual neuronal spike trains. Secondly, the spike trains are associated with the stimuli that were presented at the time of the spike. Lastly, the cells are be identified and grouped based on their response to the stimuli. In the following sections, I go into detail of how these steps are accomplished.

2.5 Neuron Finding

The offline processing of recorded voltages has been described previously (Litke et al., 2004). This processing is done using the software Vision, a custom codebase developed specifically in this lab. Briefly, on a given electrode, spikes are

identified as voltage deviations above a set threshold from the mean. Each spike is represented by a 182-element vector comprised of the voltages at that electrode and the surrounding electrodes. All spikes are transformed using the dimensionality reduction method of Principle Component Analysis (PCA) and projected into the PCA space. Spikes are then clustered into neurons with an automated clustering algorithm (Fig 2.3). Any neurons identified as contaminated (having spikes within the refractory period) are removed. Duplicate neurons are found in two ways and are also removed. Duplicates across seed electrodes are found by looking for high correlation between spike times for all neurons. Duplicates on the same seed electrode are found by comparing the electrophysiological image (EI), which is the average voltage over the array at the time of and following a spike. The EI can show general features of the cell such as approximate cell body location, size, and direction of axon.

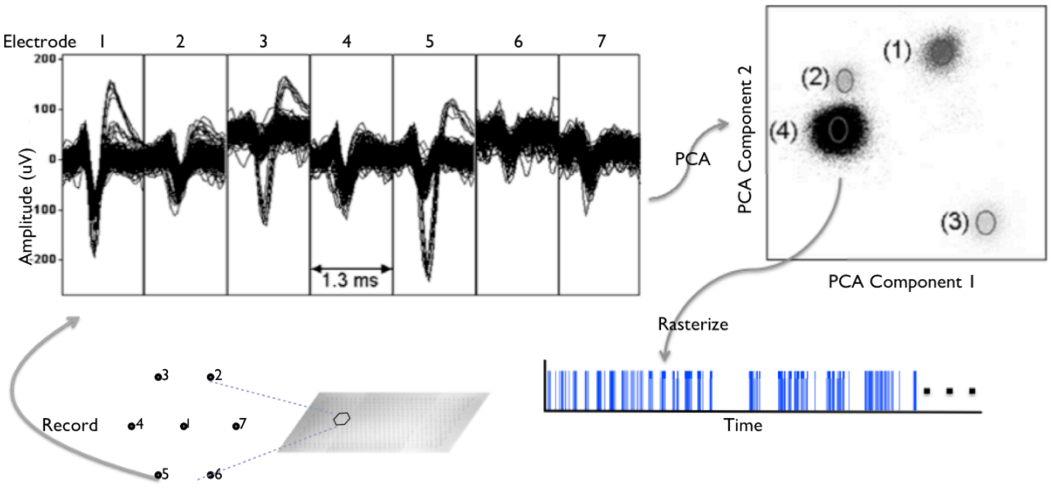

Figure 2.3: Neuron Identification pipeline. Going from a recording to spike timing data is a multi-step process. It begins by taking the raw voltages from seven electrodes and forming a 182-element vector. That vector is transformed into the PCA space and clusters are identified, many of which correspond to the spikes belonging to a single RGC. Adapted from (Litke et al, 2004).

2.6 White Noise Analysis

Analysis of the RGCs response to white noise has been described in detail previously (Sakai, 1992; Rieke, 1999; Chichilnisky, 2001). Briefly, a flickering square grid movie is shown to the entire retinal preparation. After each neuronal spike, the preceding 25 frames of the movie are flagged. Each spike-associated 25 frame clip is then vertically aligned to the other 25 frame clips, and averaged to form a single 25 frame movie that represents the mean stimulus leading up to a response (Fig 2.4A). This constitutes the spike triggered average (STA). If the spikes were correlated to a particular area of the movie, there should be a deviation from the mean luminance (for example, the average square is white if the neuron preferred the onset of light, or the average square is black if the neuron preferred the offset of light). This constitutes the Receptive Field (RF) of the neuron, which is fitted to a 2 dimensional Gaussian to denote its diameter and location. The pixels within the RF are then averaged and displayed as a function of time to create the Time Course (TC), which provides an easier way to visual the time dependency of the STAs of many neurons simultaneously (Fig 2.4B).

The time course is fitted with a sum of two filters (Petrusca et al., 2007):

$$T(t) = a_1 \left[\left(\frac{t}{\tau_1}\right) \exp\left(1 - \frac{t}{\tau_1}\right)\right]^{n_1} + a_2 \left[\left(\frac{t}{\tau_2}\right) \exp\left(1 - \frac{t}{\tau_2}\right)\right]^{n_2}$$

where t is the time before a spike, τ_n are the filter time constants, a_n are the amplitudes, and n_n are the number of stages of the filters. The fitted function provides the peaks and zero-crossings of the TC.

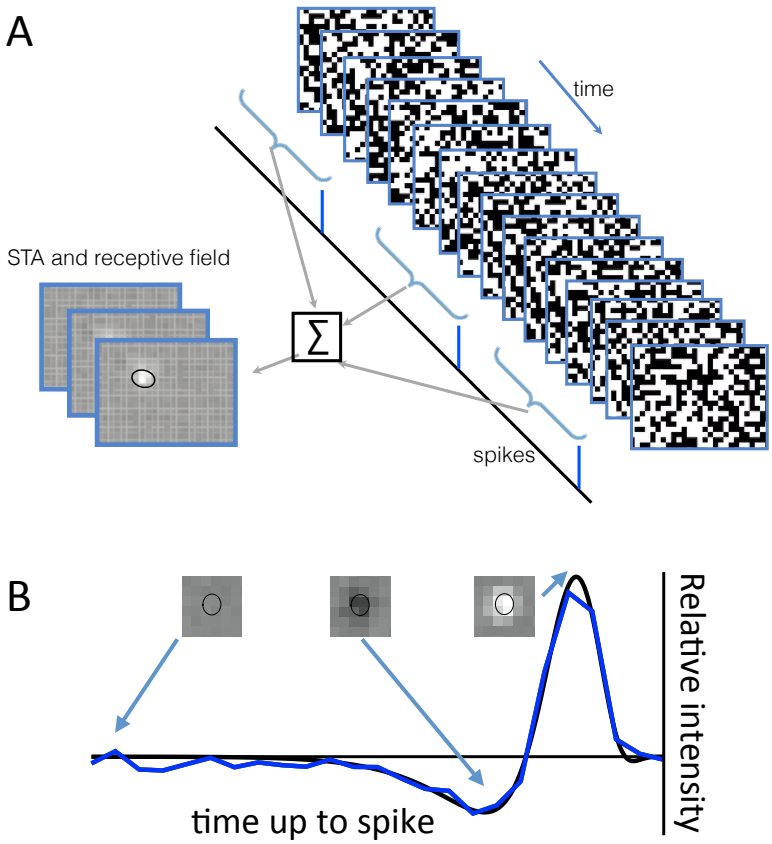

Figure 2.4: STA calculation. A) Calculation of the Spike Triggered Average provides the mean stimulus the precedes a spike, giving information on what spatial and temporal features the neuron is extracting from the visual field. B) The Time Course represents the STA collapsed to a single variable as a function of time. The blue line represents the raw data points, the black line is the fitted curve.

2.7 Direction Selectivity Analysis

The single parameter DS analysis pipeline was a custom MATLAB analysis code that I helped develop specifically for the data we acquire in our lab. Direction selective (DS) responses were calculated for each identified neuron by determining the number of spikes elicited during 5 presentations for each of 16 directions of the

drifting square wave stimulus (Fig 2.5). The spikes rates were averaged over the 5 presentations and normalized by dividing the individual spike rate at each orientation by the spike rates summed across all orientations. A single cell's response to a direction was characterized by a vector with length equal to this normalized response and the direction equal to the direction of the stimulus. Direction selectivity of a cell was then characterized by the vector sum of response vectors to all directions and called the direction selective vector of the cell. Its magnitude could vary from 0 (no direction preference) to 1 (responses to a single direction only). In addition, the Direction Selective Index (DSI) for each cell was calculated:

$$DSI = \frac{(pref - null)}{(pref + null)}$$

where *pref* is the average spike rate for the stimulus oriented closest to the direction selective vector, and *null* is the average spike rate for the stimulus 180 degrees away from *pref* (Elstrott et al., 2008). Cells with a DSI > 0.5 were classified as direction selective.

To determine tuning curve width, the cell's responses were fitted to the von Mises distribution (Oesch et al., 2005):

$$R = \frac{R_{max} e^{k \cos (x - \mu)}}{e^{k}}$$

Where R is the average spike rate for motion in a given direction, x is the given direction in radians, R_{max} is the maximum response, μ is the preferred direction in radians, and k is the concentration parameter for the tuning width. All parameters

were allowed to vary. Tuning curve width was then estimated as the full width at half height (fwhh) of the fitted curve (Elstrott et al., 2008):

$$fwhh = 2\theta$$

where

$$\theta = arc\cos\left[\frac{\ln\left(0.5e^{k} + e^{-k}\right)}{k}\right].$$

Identified DSRGCs underwent a final cut requiring total spikes in response to the preferred direction to be greater than 100, to ensure that high DSIs were not an artifact from spontaneous spikes.

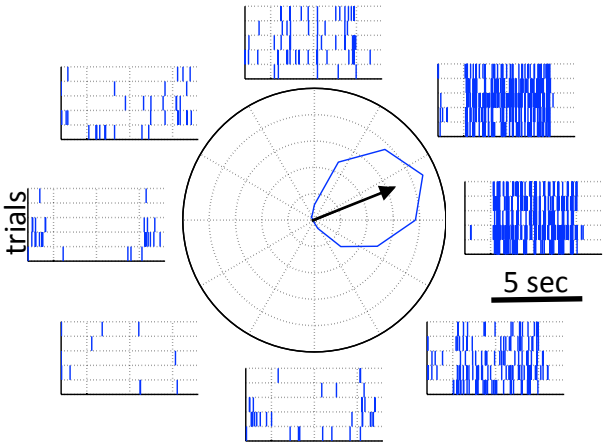

Figure 2.5: DS analysis. Raster plots show the number of spikes that were elicited for 8 of the 16 directions presented, with each row representing one of the five presentations (trials), at that orientation. A vector is drawn on the polar plot with the direction reflecting the orientation of the bars and the magnitude representing the normalized response of the spike rate in that direction.

2.8 Multi-Parameter Moving Gratings Analysis

My initial DS analysis paved the way for the DS parameter scan analysis, which processes the longer DS stimuli. In a custom MATLAB data reduction pipeline that I developed, the spikes from the randomized trials are first organized into a three

dimensional matrix, then reduced to a peristimulus time histogram to determine frequency doubling, then reduced further to the average spike rates. This 3D matrix of spike rates forms the basis for determining a cell's DS-ness, treating each spatial/temporal combination as an independent "neuron". Once each cell has its matrix of DS parameters, they are subjected to similar criteria as the single parameter DS analysis, with the added threshold that at least two spatial-temporal combinations must be considered DS. Because of the extra information provided by the multiple parameters, it is possible to use the responses to this stimulus to not only find directionality of cells, but also characterize them as ON vs ON/OFF, and look at differences in spatial and temporal tuning (Fig 2.6).

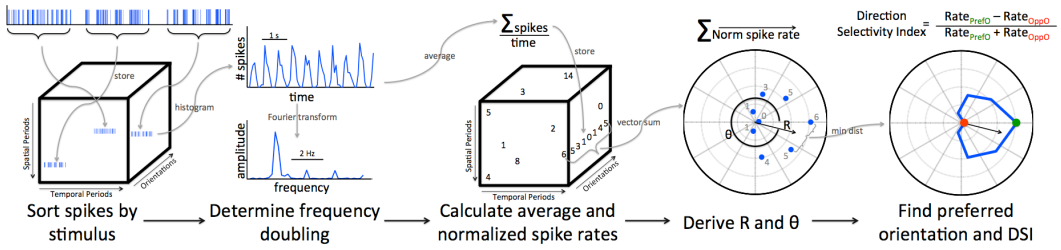

Figure 2.6: DS Parameter Scan Analysis Pipeline. Because of the many randomized combinations of direction, width, and speed of the moving bars, the stimulus must first be organized, then analyzed considering each spatial/ temporal combination as one space wherein the cell could be direction selective or not.

2.9 Full Field Flash Analysis

Full field flash response was characterized by building the peri-stimulus time histogram (PSTH) of each cell's response to the flashing intervals. The spikes from each instance of the stimulus presentation were vertically aligned and then placed into

bins, giving an improved signal-to-noise ratio on each neuron's response to the full field flashes.

2.10 RGC Functional Classification

RGCs were functionally classified according to their responses to the different visual stimulations. In general, classification is done in the PCA space, which transforms high-dimensional data to a few dimensions that encompass the majority of variance in the data. These data are then plotted on scatterplots and examined for clusters. In the case of white noise stimulation, cells were classified mainly based on the first and second principle components of the TC, autocorrelation function (a measure of intrinsic firing rate properties), and RF size (Fig 2.7A). In the case of the DS parameter scan, cells were mainly classified based on the first and second principle components of the 200-element vector containing the average spike rate to each unique parameter combination (Fig 2.7B).

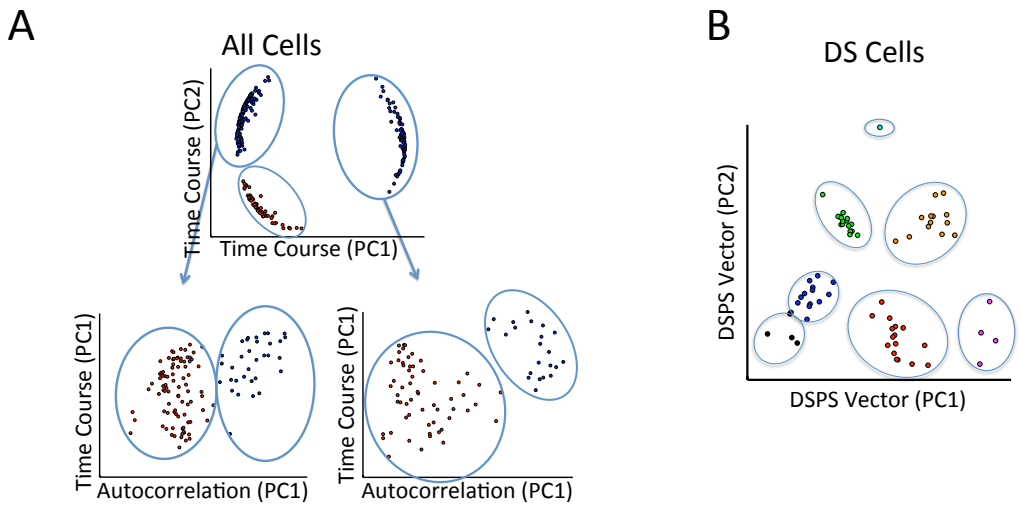

Figure 2.7: Functional classification by Principle Component Analysis. A) Classifying cells responding to white noise uses the principle components of the Time Course, Autocorrelation Function, and often Receptive Field Diameter (not pictured). B) Classifying cells responding to multi-parameter drifting gratings uses principle components of the average spike rate vector.

2.11 Channelrhodopsin Stimulation

For channelrhodopsin-2 (ChR2) stimulation experiments, all signaling to RGCs from upstream neurons were blocked with a cocktail of pharmacological blockers (Fig 2.8A) added to the Ames media (Sethuramanujam and Slaughter, 2014). DNQX (150µM) was used to block AMPA and kainate receptors such as those of OFF bipolar cells and RGCs (Borghuis et al., 2014). DL-AP7 (200µM) was used to block the NMDA receptors of some rod bipolar cells and RGCs (Brandstätter et al., 1998). L-AP4 (50µM) was used to block metabotropic glutamate receptors such as those of ON bipolar cells (Borghuis et al., 2014). Kynurenic acid (1mM) was used to redundantly block the AMPA, NMDA, and kainate receptors. Picrotoxin (50µM) was used to block GABAa receptors such as those of horizontal cells and starburst

amacrine cells. Strychnine (50μM) was used to block glycenergic receptors such as those of AII amacrine cells (Sher and DeVries, 2012).

Sparse white noise optogenetic stimulation of ChR2 expressing RGCs was then performed by projecting 16x16 high-intensity (~10 mW/mm^2), blue (450 nm) microLED array (McKendry et al., 2009). LEDs were optically reduced to 25x25 μm^2 in size and focused on the RGC layer. Frames of the sparse-white-noise LED stimulation consisted of a single LED turned on at a random position, with each frame consisting of a 50 ms-long pulse every 100 ms (Fig 2.8B). STAs were calculated similarly to those of visual responses.

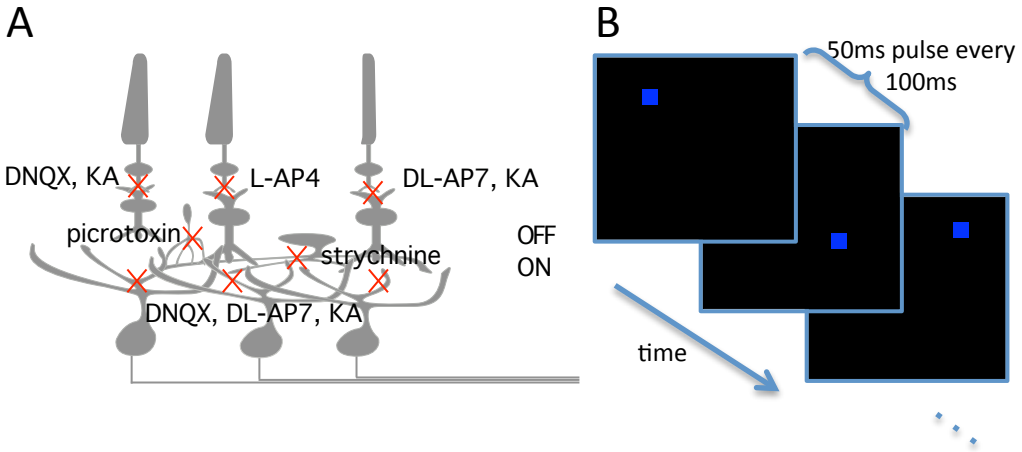

Figure 2.8: Experimental paradigm for channelrhodopsin stimulation. A) A cocktail of blockers prevents any synaptic transmission from the rods and cones through to the retinal ganglion cells. B) Stimulation for the channelrhodopsin relies on a microLED array displaying single blue pixels at high intensities.

2.12 Immunohistochemistry

In some cases, retinas were stained with PNA conjugated to Alexa Fluor 568 (Molecular Probes, L-32458) at approximately 1:50 for 5 minutes at room

temperature prior to recording so their position over the MEA could be visualized. After recording, retinas were carefully removed from the array and fixed for 30 minutes in 4% PFA. Retinas were washed in PBS (Phosphate-buffered saline) with 0.5% Triton X. Retinas were incubated for 1 day at 4°C in blocking solution (PBS plus 3% donkey serum), then incubated for 2 days at 4°C in blocking solution w primary antibodies against RFP (reactive to tdTomato) (Abcam, ab62341) and ChAT (Millipore, AB144P-200UL), or Satb2 (Abcam, ab34735) at 1:1000 dilutions. Retinas were then washed in PBS and incubated overnight in fluorescent conjugate secondary antibodies (Life Technologies, various) at 1:1000 dilutions. Finally, the tissue was washed and mounted on glass slides with Vectashield mounting medium.

2.13 Imaging

Epifluorescence and light imaging during MEA recording was done on an Olympus IX71 inverted research microscope. Post-staining epifluorescence imaging was done on an Olympus BX51 inverted microscope, courtesy of Bin Chen's lab. Confocal images were taken on the Leica SP5 Confocal microscope (60x magnification, z-stack spacing 0.34μm), maintained by Dr. Ben Abrams of the UCSC Life Sciences Microscopy Center. Images were stitched together in FIJI using the plugins for either pairwise or grid collection stitching (Preibisch et al., 2009).

CHAPTER 3: RESULTS

In this chapter I split the work of my thesis into three broad branches. In the first section, I improve our ability to functionally classify RGCs, first across different recording sessions, and second with a unique multi-parameter stimulus. In the second section, I detail work on matching anatomy with physiology. In the third section, I compare wildtype retinas to mutant retinas, first in a cell adhesion molecule knockout, and second in a developmental transcription factor knockout.

SECTION 3.1: IMPROVEMENT OF FUNCTIONAL CLASSIFICATION

This section details two projects I worked on creating novel analysis codes for the data our lab is able to collect. The first project builds off our well-established white noise dataset protocols and looks for a way to better match cell types found in different experimental preparations. The second project involves an in-depth analysis for moving grating stimulation.

3.1.1: White Noise Classification Across Preps

Introduction

In mammals, RGCs are a heterogeneous population, with each type thought to encode a different aspect of the visual scene. Many decades of research have been dedicated to studying the function of RGCs, in order to parse out what the characteristics of these different populations could be and how they might differ from each other (Kuffler, 1953; Oyster and Barlow, 1967; Van Wyk et al., 2009; Baden et

al., 2016). However, we need to be able to consistently identify true RGC types in our functional classifications, so that they can be correlated with anatomically identified cell types and with molecular markers. Without a comprehensive understanding of wildtype RGCs, we cannot effectively explore the changes in knockdown or disease-model mouse circuitry.

The MEA is an excellent tool for functionally identifying and classifying many different physiological RGC types. It has been used successfully on retinas in primate (Chichilnisky and Kalmar, 2002; Field et al., 2007; Petrusca et al., 2007; Gauthier et al., 2009), rabbit (Devries and Baylor, 1997), ground squirrel (Sher and DeVries, 2012), rat (Anishchenko et al., 2010), and mouse (Elstrott et al., 2008). In particular, the white noise stimulus has seen a great deal of success, as it can simultaneously stimulate many RGCs, both ON and OFF types alike, and provide a reasonable estimate of each cell's area of sensitivity in the visual space (receptive field, or RF) and mean preferred stimulus that elicits a spike (spike triggered average, or STA) (Sakai, 1992; Rieke, 1999; Chichilnisky, 2001).

A major difficulty that comes up in this work is identifying similar types across preparations. Many studies pool cells together (Farrow and Masland, 2011; Baden et al., 2016) in order to get enough cells to successfully do statistics on, which can introduce a layer of variability between preparations. Issues such as the health of the retina, age of the mouse, variations in pressure while pressing the retina onto the array, and minor variations in temperature during the experiment can potentially contribute to systematic differences between cell types in two different retinas that

should be fundamentally identical. To counteract this problem, my project begins by performing classification of RGCs within each retina individually. Once classes were established, their properties were averaged to form a single "super-neuron" that represents the entire class. These super-neurons are normalized to one well-established class in each preparation, in an attempt to remove any systematic variation introduced in the recording. Finally, super-neurons from many different retinas were grouped together in a "super-retina" and classification was performed again. If two super-neurons that came from different retinas were classified together, we could conclude that those two cell types were the same in both retinas.

Results:

RGC responses were measured by placing an isolated wild type mouse retina on a 512-electrode array and projecting various visual stimuli, such as spatio-temporal white noise and full field flashes, onto the photoreceptor layer. Action potentials from hundreds of RGCs were identified in a single retinal preparation. Classification of RGCs within a single retina was based on their functional properties such as the STA response to white noise stimulus, and PSTH to the full field flashes. Principal Component Analysis was used to extract features of the response most useful for classification. Spatial organization of the receptive fields was not taken into account in the classification process. And the end of the processing for a single retina, many classes were found based on similarities in their time course (TC),

autocorrelation function (ACF), receptive field diameter (RF), and full field flash response (FR) (Figure 3.1).

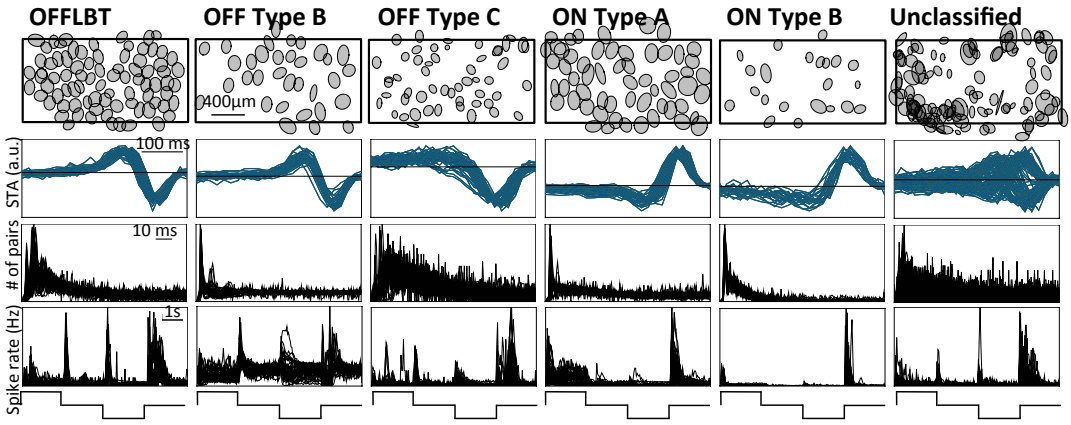

Figure 3.1: A single retina classified using white noise and full field flashes. Note that the receptive field mosaic arrangement was not used as a criteria for classification, and that it is purely a consequence of grouping cells with similar response properties. This particular retina had RGCs that sorted into five cell types, consisting of three OFF types and two ON types, as well as a population of cells that were considered "Unclassified". Unclassified cells were either too weakly responding to be assigned one of the established classes, or too sparse to be confidently put in their own class.

In this study, we recorded from 6 different wildtype retinas. The area recorded from and recording procedures were kept as consistent as possible. All retinas had strong responses to stimuli and no obvious defects in terms of health. However, visual inspection was not enough to say one RGC was in the same class as an RGC from a different retina, or even that a class of RGCs was the same as another class of RGCs found in a different retina (Figure 3.2). There were still often systematic differences in simple variables such as RF diameter, the response latency (RL), which is defined as the time where the TC crosses zero, and the degree of transiency (DOT), which is defined as:

$$\left|1 - \frac{|area_1 + area_2|}{|area_1| + |area_2|}\right|$$

where $area_1$ is the integral of the TC prior to the zero crossing, and $area_2$ is the integral of the TC after the zero crossing. A DOT of zero implies a monophasic TC, which corresponds to sustained spike responses, and a DOT of 1 implies a biphasic TC, which corresponds to transient spike responses.

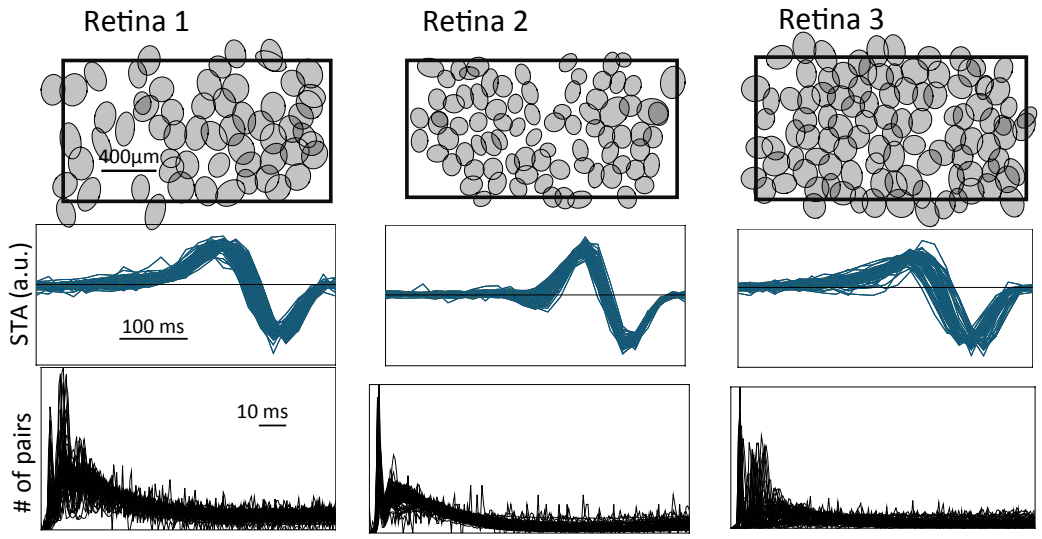

Figure 3.2: Three example classes from three different preparations. Although evidence suggests these three cell types represent physiologically identical RGCs but in different retinas, variation in preps make it difficult to confirm.

Within a single retinal preparation, spacing and completeness of the RF mosaics are used as a control during classification. In many cases we see high variation across at least one parameter even within one type, such as the RF diameter. This means that pooling RGC data from all retinas in order to identify cell types across multiple preps is not feasible. Thus each type within one retina is averaged in order to represent that cell type in that retina (Figure 3.3).

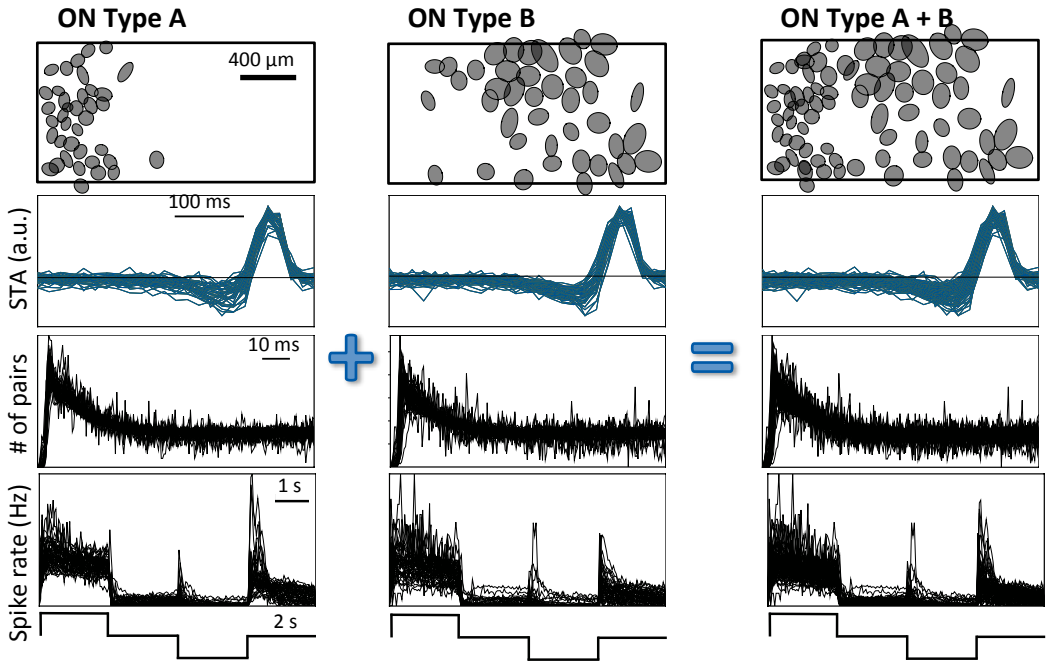

Figure 3.3: Averaging accounts for in-retina differences. Consider two naïvely classified cell types, labeled here A and B, which were likely separated due to differences in the receptive field size. Combining the two classes shows almost no differences in TC, ACF, or FR, and a complementary RF mosaic patterning, bringing their initial separate classifications under suspicion.

Once RGC classes were averaged, we tried to account for systematic differences between the retinas. Thus for every RGC type in each retina, we calculated that type's normalized RF and its scaled TC function using the Response Latency. Normalization was to an "anchor" type (OFFLBT) in each retina that was consistently identified by eye (Figure 3.4). Thus, all OFFLBT cell types from every retina were assumed to have the same RF and RL, and all other classes were sized relative to that. This hierarchical naming convention is used throughout this project, and goes as follows: 1) the cell type's polarity, either ON or OFF, 2) the cell type's RF diameter, either large (L), medium (M), or small (S), 3) the cell type's recency of TC zero crossing, either brisk (B) or sluggish (S), 4) the cell type's DOT, either

transient (T) or sustained (S). Although this normalization step was done blind to any cell types save OFFLBT, post-classification coloring (see Fig 3.5) is given to show that the normalization did result in a better separation of classes. For example, the difference in two OFF cell types' RF diameters as measured by a Student's t-test went from p = 0.0651 to p = 0.0122 (Fig 3.4A) and the difference in tow ON cell type's RL went from p = 0.0747 to p = 0.0337 (Fig. 3.4B).

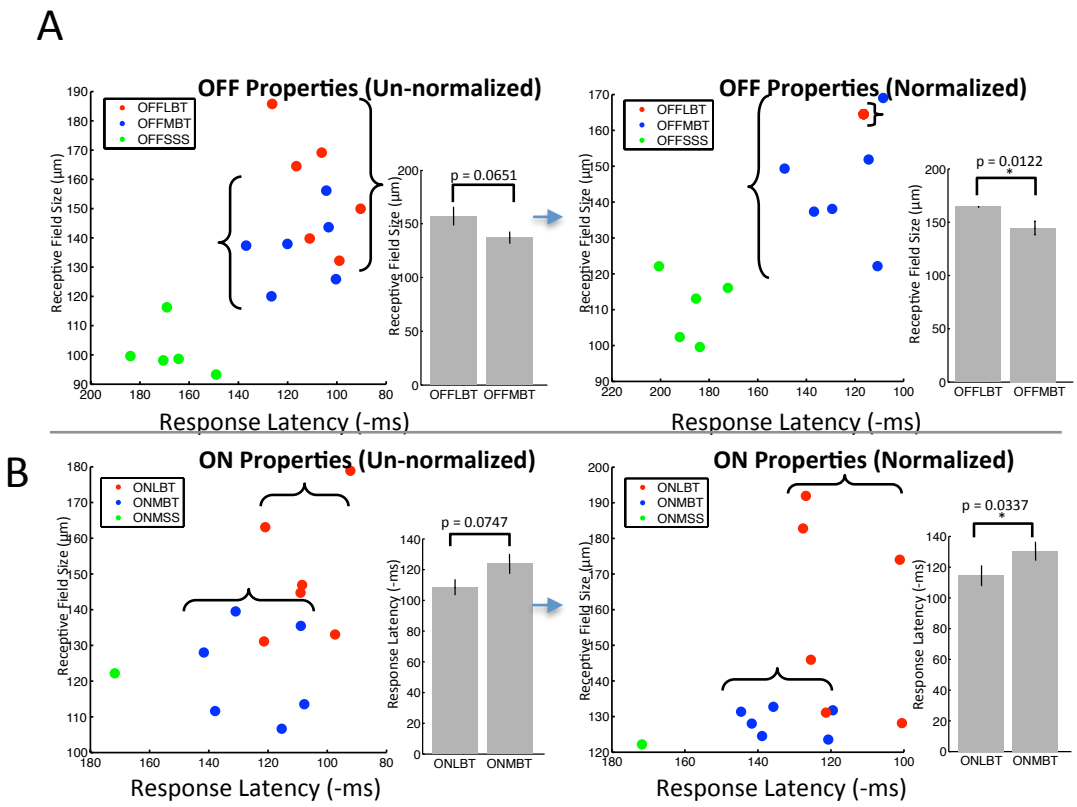

Figure 3.4: Normalization decreases across-retina differences. For each retina, the OFFLBT cell type is used as the "anchor" class and the other cell types are normalized to it. This improves the differentiation between types.

PCA classification was done on the averaged types, treating them as one "super-retina" composed of "super-RGCs". Here, RF mosaics cannot be used as a

check, instead, we ensured that no two types from one retina were classified together. The initial simplest classification was, as always, the ON types and the OFF types, and were thus split apart in a previous classification step. Many different projections were available for classification, as the first two principle components of the TC, ACF, (Figure 3.5). We found that all the super-neurons from the 6 retinas could be grouped into 5 consistent classes and one outlier class that was found in only one retina. These classes were named according to the convention as OFFLBT, OFFMBT, OFFSSS, ONLBT, ONMBT, and ONMSS.

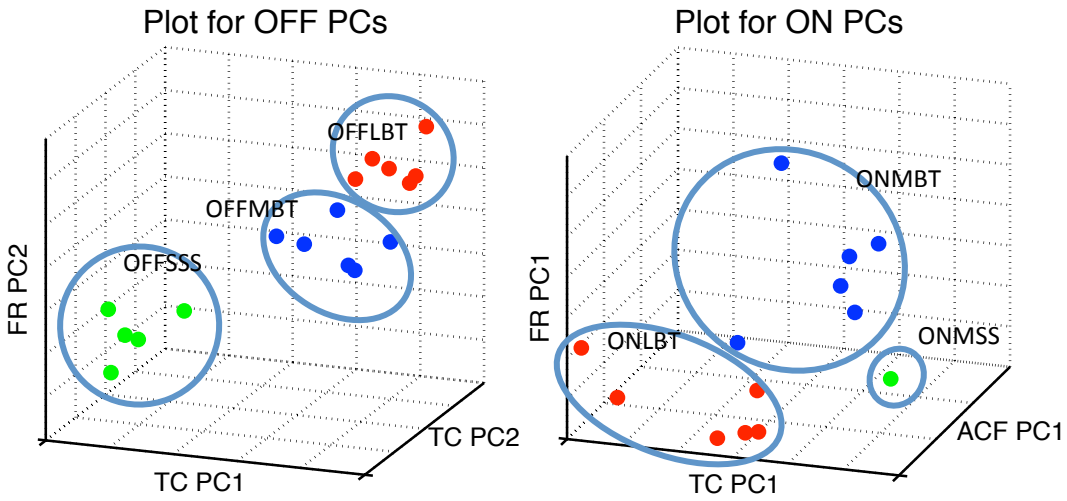

Figure 3.5: Classification of super-neurons into super-classes. The averaged celltypes from all retinas (super-neurons) were classified using a method very similar to the one used to classify neurons in a single retina. The ON and OFF types were easily separated and thus presented in different plots, and these 3D projections of Principle Components (PCs) show that a combination of the TC, ACF, and FR can separate these into types nicely. An iterative approach was taken to ensure that no two super-neurons in one class came from the same retina.

Finally, all the super-neurons were plotted together to verify the results of the higher-level classification (Figure 3.6). Each graph shows the same cell type in each

retina recorded from, separated by an arbitrary vertical distance for clarity. Plotting them in this manner allows for visual inspection of some inconsistencies. For example, in the TC of the second retina from the top (maroon trace) it can be seen that in every cell type, there is a more equally biphasic shape to the TC. It can also be seen in the ACFs of the fifth retina from the top (dark green trace) that there is not a sharp spike early on, implying that this retina had less bursty responses, but that this was consistent across cell types (Fig 3.6). In addition to the function of time variables, we also noted the simple variables:

For OFFLBTs, RF = 156.9 ± 8.1, RL = -108.2 ± 5.2, and DOT = 0.93 ± 0.02.

For OFFMBTs, RF = 136.8 ± 5.2, RL = -115.3 ± 6.1, and DOT = 0.81 ± 0.04.

For OFFSSSs, RF = 101.2 ± 3.9, RL = -167.3 ± 5.6, and DOT = 0.66 ± 0.03.

For ONLBTs, RF = 149.6 ± 7.5, RL = -108.2 ± 4.9, and DOT = 0.86 ± 0.03.

For ONMBTs, RF = 122.5 ± 5.6, RL = -123.8 ± 6.1, and DOT = 0.93 ± 0.03.

For ONMSSs, RF = 122.2 ± 0, RL = -171.8 ± 0, and DOT = 0.71 ± 0.

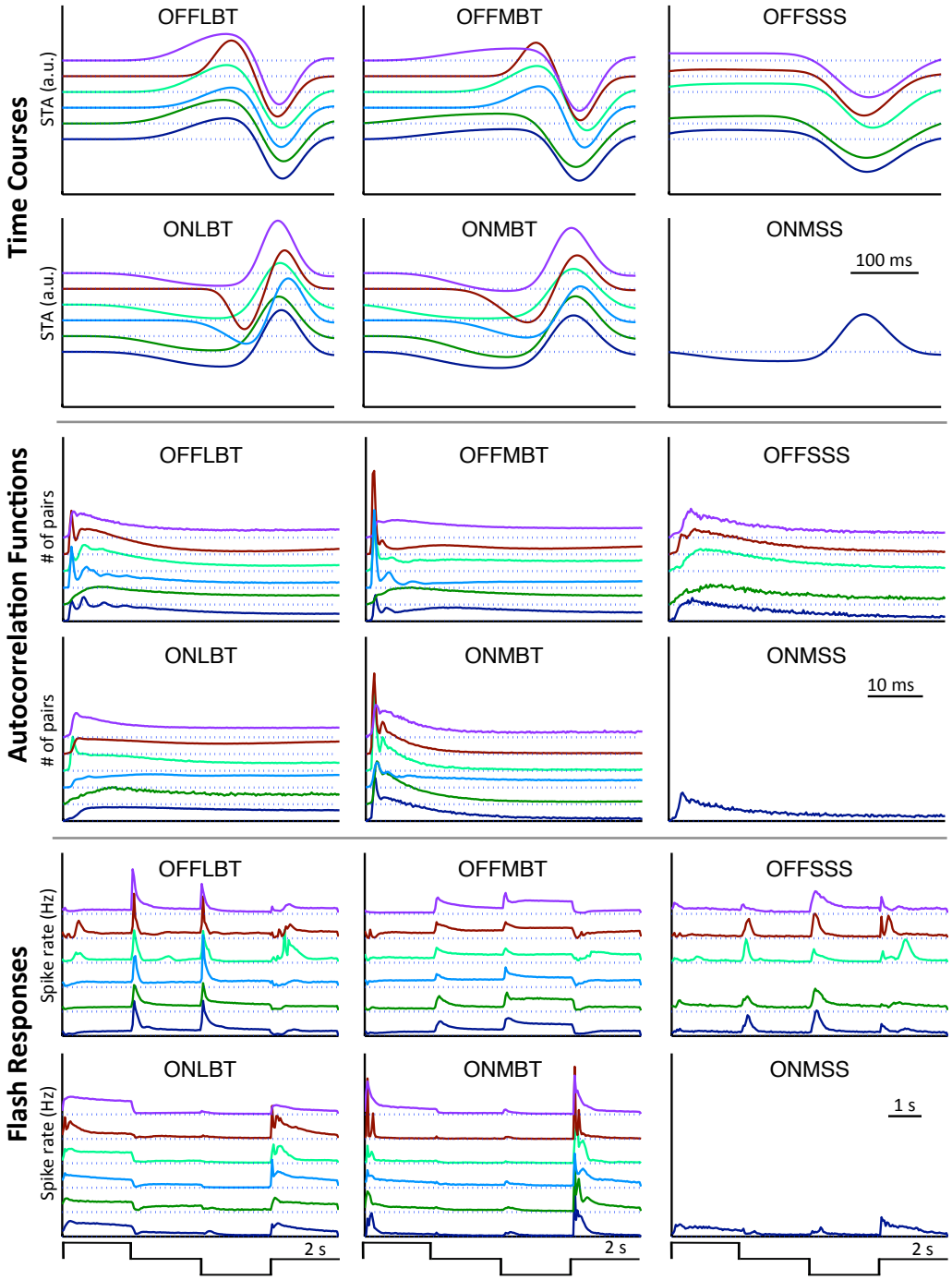

Figure 3.6: Final classifications of all retinas. In this figure, all of the "super-neurons" time dependent features (TC, ACF, FR) are plotted, organized into graphs by cell type, and colored by retina of origin. The traces are all separated by an arbitrary vertical distance so comparisons can more easily be made.

Discussion:

Our data shows that five individual RGC types can be consistently identified in wildtype mouse retinas and that this identification can be done exclusively through their response properties to visual stimuli. These cell types include ON and OFF RGC types with distinct spatio-temporal filtering properties. Furthermore, we find that individual cell types' receptive fields tile the retina in a regular mosaic pattern. We show that RGC types in the mouse have distinct functional properties, which are consistent across different retinas. Although there is some retina-to-retina variability, a combination of averaging and normalizing was able to show that even across retinas, a cell type in one retina is more similar to an analogous cell type in a different retina than it is to other cell types in its native retina. This indicates that each RGC type represents a distinct retinal circuit that sends information about a particular aspect of the visual scene to the brain.

There are many reasons why pooling neurons from different recordings can lead to over-classification. As previously mentioned, any differences in health, age, or experimental preparations of the retina can cause systematic differences between two sessions of recording. However, there are also purely biological factors that can be confounding to a naïve classification. For example, it has been shown anatomically that there are intra-retina gradients of cell dendritic arbor size in certain RGC subtypes (Bleckert et al., 2014). There are also intra-retina gradients of opsin expression in the mouse cone population, which can create differences in the color sensitivity of functionally identical RGCs (Haverkamp et al., 2005). For these

reasons, finding cell classes first in a single retina and using receptive field mosaics as a control provides much more confidence that a group of cells might constitute a single cell type.

The presented functional characterization and classification will be valuable for investigating retinal function and development. It provides a necessary control and a toolbox for identifying changes of the complex retinal structure and function in genetically manipulated mice. This technique could be applied to recordings done in any of the animal models used for MEA recordings, such as monkey, rabbit, squirrel or rat, as well as mutant models of mouse.

3.1.2: Population-Level Functional Characterization of Direction Selective Mouse Retinal Ganglion Cells

Introduction:

Certain RGC types, collectively called direction selective retinal ganglion cells (DS RGCs), respond to motion in one direction and are suppressed by motion in the opposite direction. This phenomenon is a remarkable emergent property of the retinal neural circuits. The purpose of this study is to characterize these cells' spatial and temporal response properties at the level of complete populations. DSRGCs have long been looked at as a beautiful example of retinal circuitry (Barlow and Hill, 1963; Barlow et al., 1964; Weng et al., 2005). For some time it has been known in rabbit that there are at least two major types of DS cells – an ON/OFF type that responds to

fast motion, and an ON type that responds to slow motion (Oyster et al., 1972). There are four ON/OFF types that correspond to the cardinal directions on the retina (Oyster and Barlow, 1967), and are thought to be involved in visual response (Cruz-Martín et al., 2014). Conversely, there are three ON types that correspond to the orientation of ear canals (Oyster and Barlow, 1967; Dhande et al., 2013) and are thought to be involved in the optokinetic response (Yonehara et al., 2009). Other studies of DS cells has provided evidence for an OFF type (Kim et al., 2008) a second set of ON types (Kanjhan and Sivyer, 2010; Hoshi et al., 2011) and more than one ON/OFF type in the nasal direction (Rivlin-Etzion et al., 2011).

Since then, mouse studies have looked at these cells in terms of their molecular markers and labeled cell lines (for review, see (Wei and Feller, 2011)). The DRD4-GFP mouse line labels nasal selecting DS cells (Huberman et al., 2009). The TRHR-GFP mouse line also labels nasal selecting DS cells, although it is not clear if this is the same or different population as DRD4-GFP (Rivlin-Etzion et al., 2011). A final described mouse line that labels nasal selecting DS cells is the W9-GFP line (Kay et al., 2011a). The HB9-GFP mouse line labels downward selecting DS cells (Trenholm et al., 2011), as does the BD-GFP mouse line (Kay et al., 2011a). The Hoxd10-GFP mouse line labels the ON DS cells, as well as the temporal selecting ON/OFF DS cells (Dhande et al., 2013). Other molecular markers have been identified, such as Cad6, which labels subsets of ON/OFF DS cells, and CART, which labels all ON/OFF DS cells (Kay et al., 2011a). Thus there is some controversy

as to whether mice have the seven classically described DS RGC types, or upwards of 12 DS RGC types.

In this study, we utilize a multi-electrode array (MEA) to record from hundreds of mouse RGCs simultaneously. This allows us to record from multiple DS RGCs, while maintaining information such as the relative angles of stimuli the cells respond to, and the relative location of cell receptive fields. We are also able to show a very extensive stimulus, providing information regarding the tuning of these cells that we believe is more comprehensive than any other study has to date. We find that in a given retina, we can detect seven types of DS cells consistently, four ON/OFF and three ON. We find that spatial/temporal tuning of the ON/OFF cells vary between directions, and that while ON/OFF types show consistent relative angle preferences, the ON types can vary widely. We also find that for DS RGC types that consistently map to the white noise stimulus, their receptive fields tile the visual space.

Results:

Wildtype mouse retina was isolated and placed on a 512-electrode array to record RGC spiking activity. To measure direction selective responses, full field drifting gratings were shown at a variety of spatial and temporal periods. Additional visual stimuli such as spatio-temporal white noise and full field flashes were presented as well. A single recording yielded action potentials from hundreds of RGCs. Identified RGCs were classified as either “DS” or “non-DS” based on a normalized difference between the cell’s firing rate in response to its preferred

direction versus the opposite one (Direction Selective Index, or DSI, see Methods). They were also required to have a mean spike rate of at least 2 Hz (Fig 3.7A). After the initial thresholds, the passed cells were examined manually for cells that were clear false positives (Fig 3.7B).

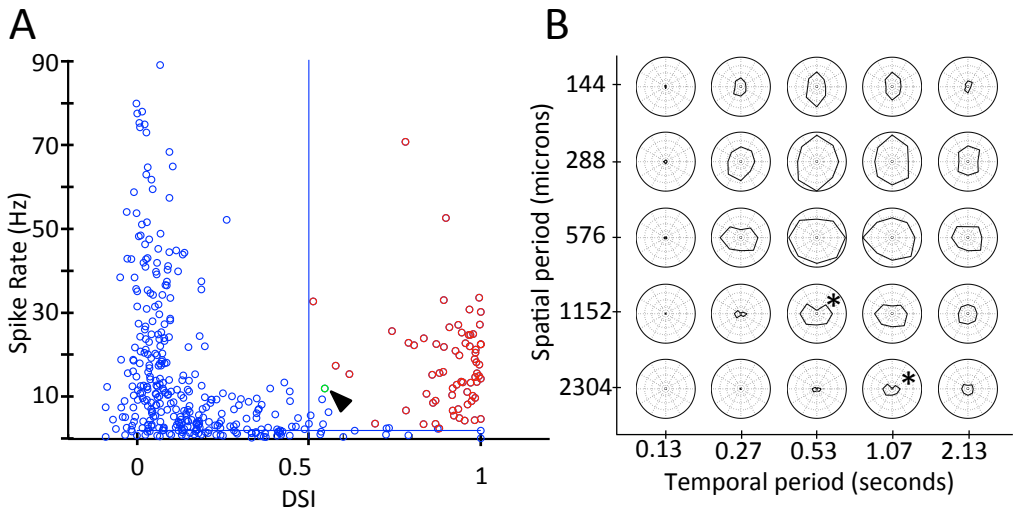

Fig 3.7: Determining the DS cells in a population. A) The criteria for the first threshold of determining DS cells is to have a spike rate over 2Hz, and a DS over 0.5 (blue horizontal and vertical lines). After this, every cell is manually inspected. Blue dots represent cells that failed either threshold, red dots represent cells that passed both thresholds. Blue dots that are to the top and right of the blue lines represent cells that passed the automatic threshold, and failed the manual examination. The green dot with an arrowhead is the cell shown in B. B) A cell that passed automatic thresholds, but failed manual inspection. Asterisks indicate the spatial temporal periods that met the automatic criteria, but on inspection, it is unlikely to be a true DS response.

In each preparation, every recorded cell was presented with 8 directions of full field moving gratings, at 5 different spatial periods and 5 different temporal periods, for a total of 200 unique stimulus combinations. Many cells had responses that were invariant to direction, showing only a differential spike rate in response to spatial and temporal changes (Fig 3.8A), which is the expected response pattern of a non-DS cell.

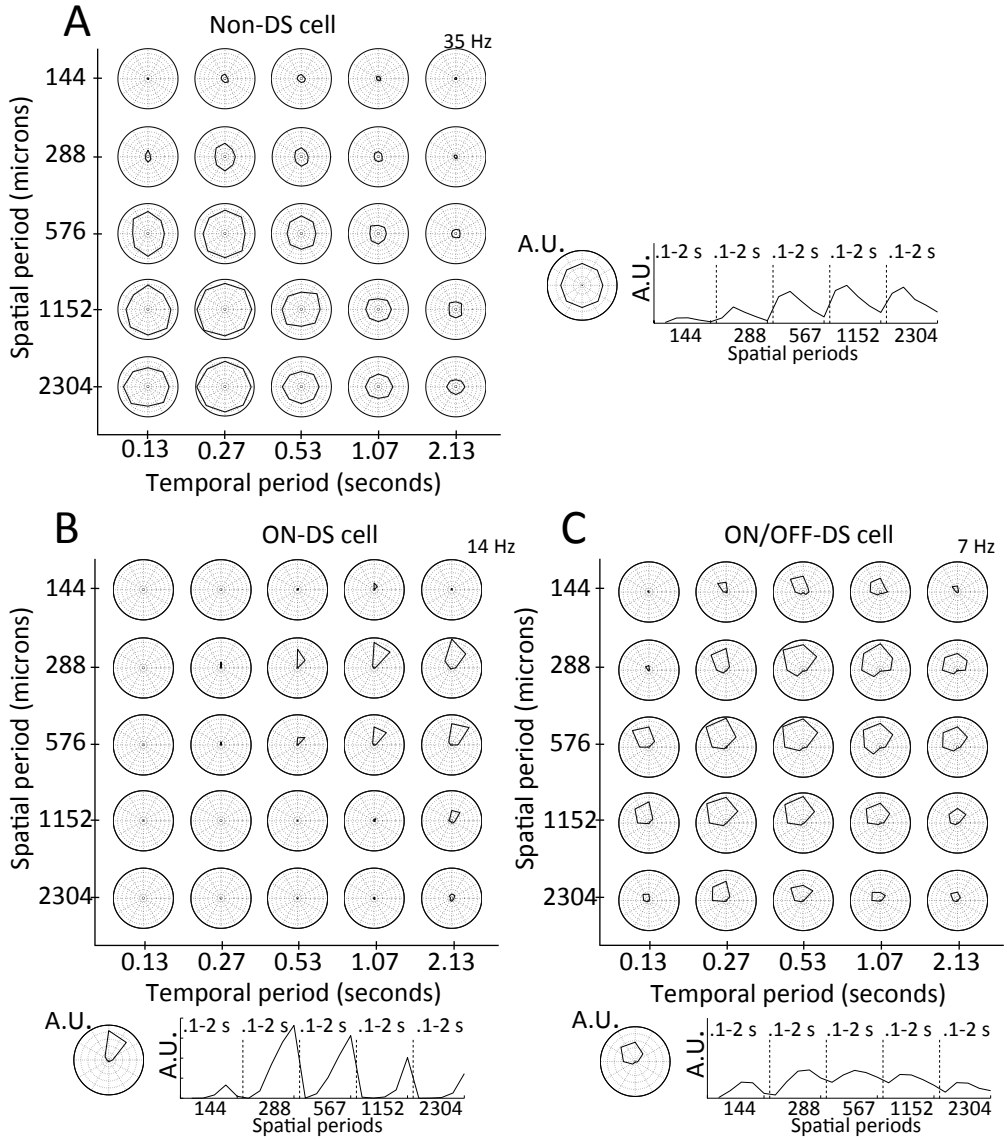

Fig 3.8: Examples of responses to DS parameter scan stimulus. All panels show first an array of 25 polar plots, showing each cell's average response to the combination for 5 spatial periods, 5 temporal periods, and 8 directions. Below each the 5x5 plot shows a simplified version, with the polar plot averaging the 5x5x8 dataset along the directional vector, and the linear plot showing a arbitrarily arranged 25-element vector of the cell's mean response as a function of spatial/temporal periods. A) An example non-DS cell, with a preference for relatively fast motion and no directional preferences. B) An example ON DS cell, with a preference for slow movement and narrow directional tuning. C) An example on an ON/OFF DS cell, with broad spatial/ temporal and directional tuning.

For the cells identified as direction selective, they often showed a highly consistent directional tuning, in addition to a clear gradient of spatial-temporal tuning. The ON DS cells tended to have the highest responses in the longest temporal periods (that is, for any given bar size, those cells preferred the slowest speed they traveled) and also had relatively narrow directional tuning (Fig 3.8B). The ON/OFF DS cells tended to respond to a much broader variety of spatial and temporal combinations, peaked around 0.5-1 second temporal periods, and also tended to have more broad directional tuning (Fig 3.8C).

In this study, we recorded from a total of 2723 neurons, and of those 426 were identified as direction selective. This came out to approximately 15% of recorded cells in each preparation that displayed clear DS characteristics (Fig 3.9A). This was fairly consistent across healthy recordings. After cells were identified as DS, they were further classified into subsets based on their directional, spatial, and temporal tunings. This was done independently in each preparation to try and prevent as much as possible over-classification from inter-prep variability. We generally could identify up to 7 distinct types per retina based on their directional, spatial, and temporal tuning, which seemed to correspond to 4 ON/OFF types, and 3 ON types (Fig 3.9B). We saw that in general, the ON/OFF type DS cells were found more robustly than ON type.

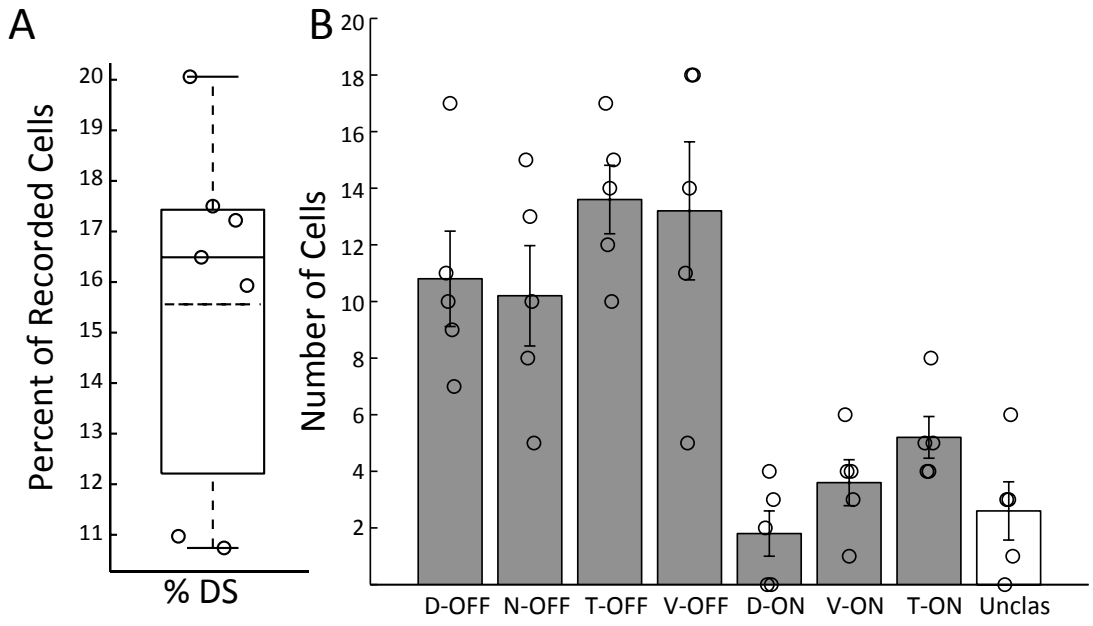

Figure 3.9: A consistent fraction of recorded cells are DS. A) The average percent of DS cells is 15.3% (dotted line). Boxplot shows median (center line) 25/75th percentile (edges of box) and 0th/100th percentile (whiskers). Dots show individual data points from separate retinas. B) Similarly, we record from similar numbers of each DS subtype, and consistently detect fewer ON DS cells than ON/OFF DS cells. There is also often an "Unclassified" group of DS cells, (0-6 per retina) that don't fall neatly into any of the 7 named subtypes. Note that this graph shows the raw number of DS cells, rather than dividing by the total number of recorded cells. Because healthy recordings generally have similar numbers of total cells recorded, showing the raw numbers provides similar information, and gives and idea of typical sample sizes.

Once the classes in each preparation were established, we briefly examined the relative angles between the average vectors of each class. After alignment of the retinas based on the recording location and axon direction, we averaged each subclass's directional vector. We saw that there was a wide range of orientations not only relative to the axis of the retina (for example, the "ventral" selecting ON/OFF DS cells didn't always point exactly ventrally) but also relative to each other (for

example, not every “ventral” ON DS was 120° from the “temporal” ON DS population) (Figure 3.10A). Further analysis showed that the relative angles of DS cell types preferred direction vary by location in the retina. Different retinas showed variation in both the relative angle and absolute angle of average preferred direction for each class. We observed that more medial pieces (in this case they also correspond to “more dorsal/ventral”) showed more equal spacing (that is, closer to 120°/120°/120°) between the ON type DS cells. ON/OFF types always showed close to 90°/90°/120° separation (Figure 3.10B).

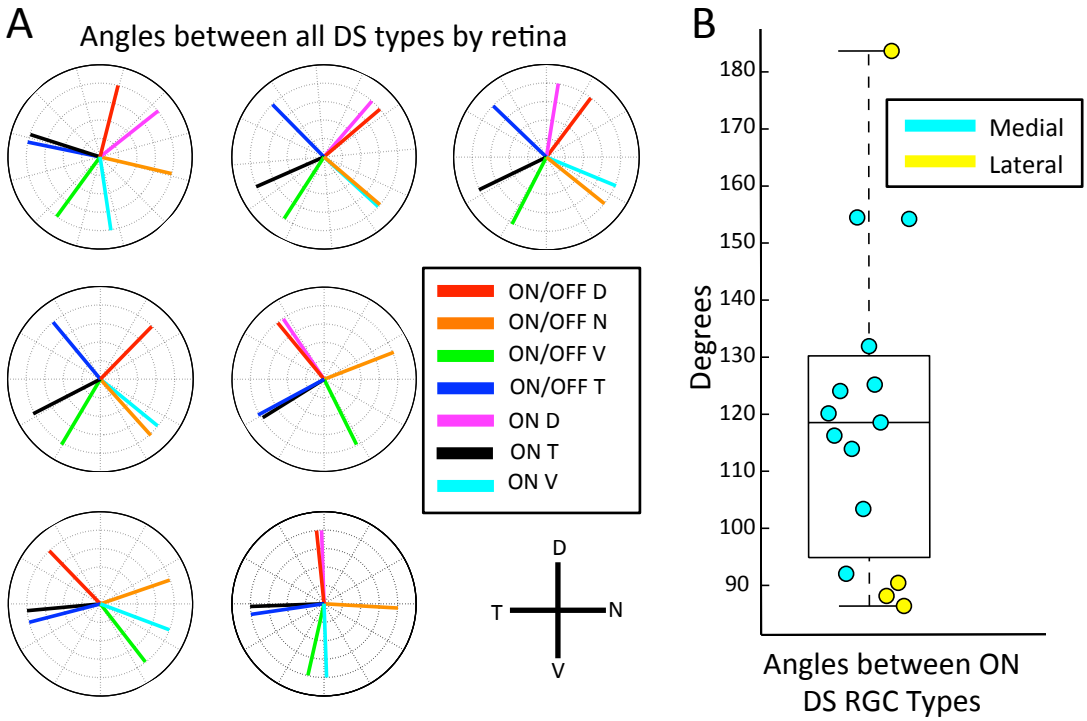

Figure 3.10: Angles between DS subpopulations are not consistent. A) Each polar plot represents a single retinal preparation, with vectors representing the average directional preference for each subclass. Each subclass is represented by a different color. Different recordings can vary greatly in terms of angles relative to the retinal coordinates, as well as angles relative to the different DS subpopulations. B) Separating recordings by location on the retina, either medial (cyan) or lateral (yellow), show that there is some correlation between location of recording and angles between DS subpopulations. Medial recordings tend toward an "even" distribution of ON DS cells (120°/120°/120°) while lateral recordings tend to have more of a (90°/90°/180°) distribution.

Once DS RGCs were identified, we next looked at these cells' responses to visual white noise and full field flashes. This type of stimulus gives information regarding the cells' receptive field and STA, and again, can provide mosaic tiling information as long as only a single preparation is analyzed at a time. To illustrate, we considered two retinas with full characterizations, displaying the

spatial/temporal/directional tunings and autocorrelation function, as well as the cells' white noise Time Course, and Receptive Field, and the full field flash peristimulus time histogram. We found that for many of the DS RGC subpopulations, in particular the ON/OFF populations, their receptive fields tiled the visual space (Fig 3.11A). Interestingly, the ON DS cells showed barely any responses to the white noise stimulus. When we tried using a white noise that updated at half the speed of the previous one (30 Hz instead of 60 Hz frame rate), we found that the ON DS cells sometimes showed a very weak ON STA (Fig 3.11B).

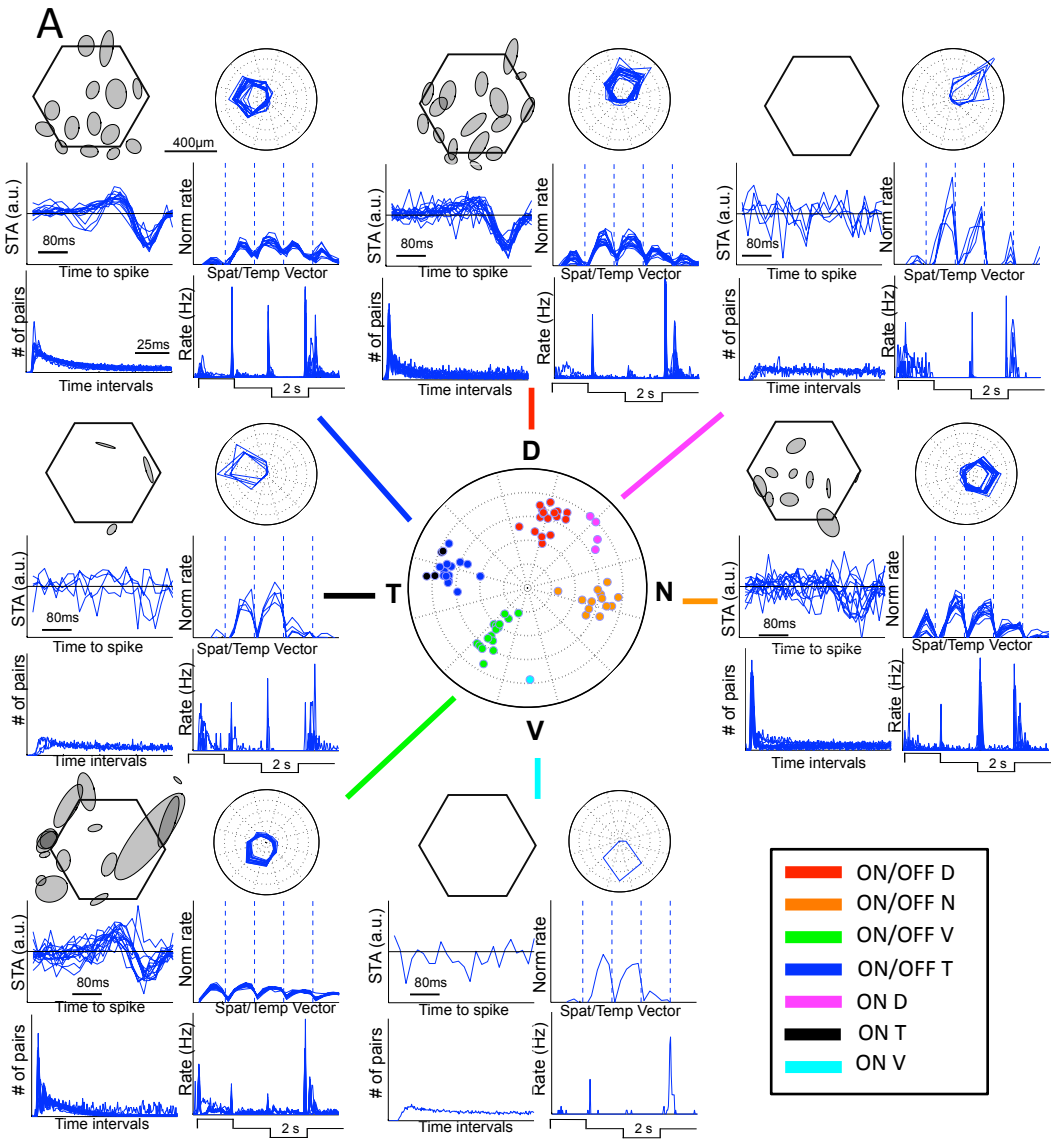

Figure 3.11: Continued and captioned on following page.

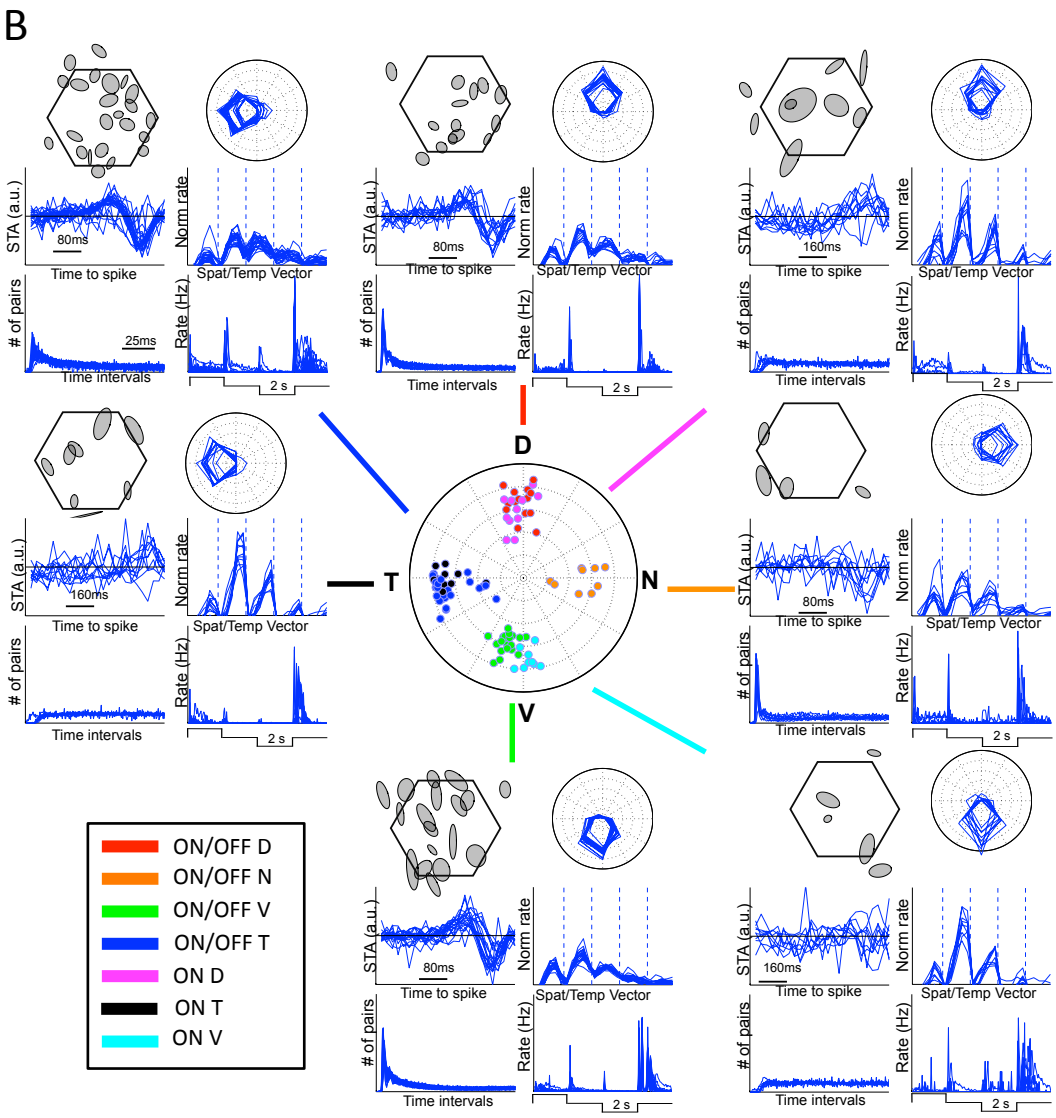

Figure 3.11: Two example retinas. A) A medial retina recording with white noise stimulation run at 60Hz. B) A lateral retina recording with white noise stimulation run at 30Hz. For both retinas, the center polar plot represents all DS cells detected in that retina, with every point representing a single cell as a vector whose angle and radius corresponds to the cell's direction and strength of DS response. The colors indicate cells of a particular subpopulation, and the line of the corresponding color connects to 6 plots which further characterize that subtype. The top left plots show the receptive field mosaic for that subtype. The top right plot shows the mean directional responses. The middle left plot shows the white noise STAs. The middle right plot shows the 25-element spatial/temporal vectors. The bottom left plot shows the ACF. The bottom right plot shows the full field flash responses.

Finally, we took some preliminary observations regarding DS RGCs' responses to speed. The speed of the bar or grating across a visual receptive field has long been used as a parameter to characterize DS cells. In our stimulation paradigm, speed can be constructed from the two parameters used in our stimulus, spatial period (the width of one grating) and temporal period (how long it takes for one grating to pass a given point). Thus in our 5x5 spatial/temporal parameter space, there are 9 apparent speeds with varying degrees of redundancy. In general, smaller spatial periods will have slower motion, and larger spatial periods will have faster motion (Fig 3.12). We saw that the ON DS cell subpopulations tended to have a very similar speed tuning that was very distinctive from all ON/OFF DS cells (Figure 3.12A). In the ON/OFF DS cell subpopulations, we saw that some cells, such as dorsal and temporal selecting ON/OFF DS cells, seemed to have no dependence on the speed of the gratings, while some cells, in particular the ventral selecting ON/OFF DS cells, showed a strong speed tuning independent of the speed's spatial/temporal construction (Figure 3.12B).

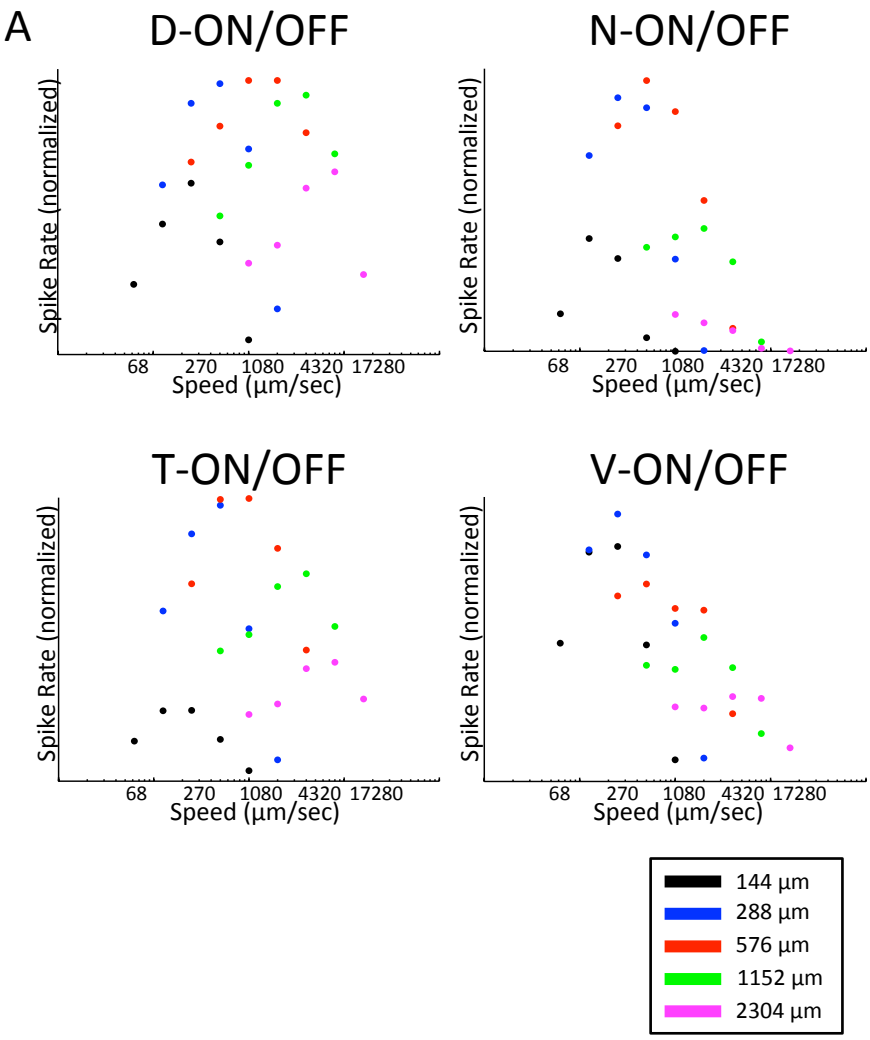

Figure 3.12: Continued and captioned on following page.

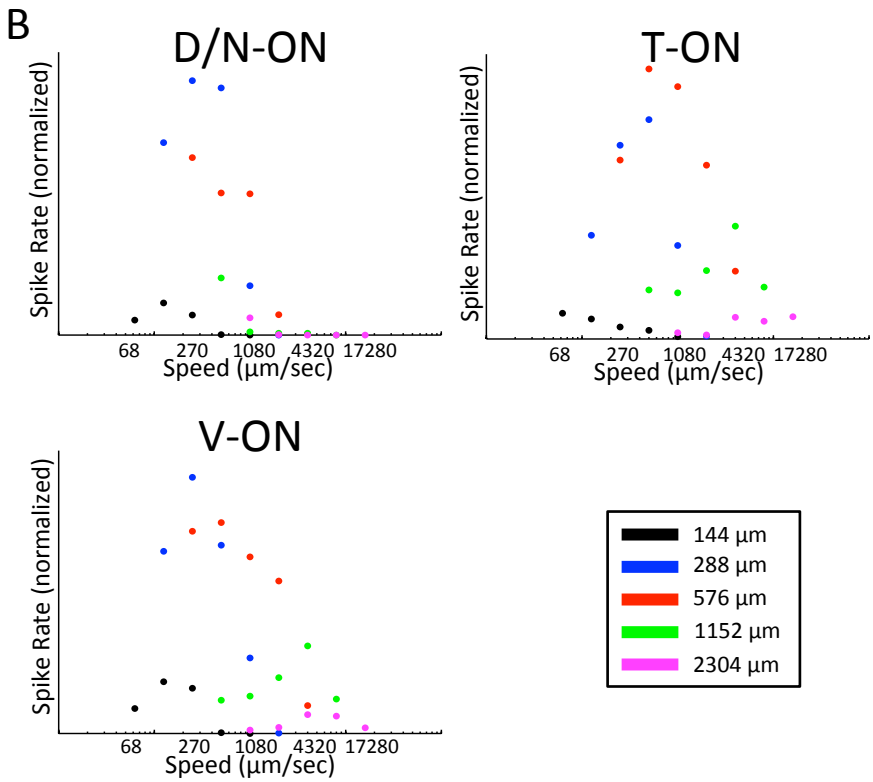

Figure 3.12: Speed tuning for different cell types. A) Typical examples of ON/ OFF DS tuning curves for the four directional subtypes found in our recordings. B) Typical examples of ON DS tuning curves for the three direction subtypes found in our recordings. Points are colored by spatial period, thus each color shows 5 points, with black points representing the slowest speeds (smallest bars at all temporal periods) and pink points having the fastest speeds (largest bars at all temporal periods).

Discussion:

Using the MEA system, we were able to record from hundreds of cells in a single retinal preparation simultaneously. This powerful technique allowed us to examine large populations of DS cells while preserving RGCs' relative relationship to one another, which can be lost when pooling data from multiple retinas. Using 7 retinas from C57/Bl6 adult mice, we examined DS RGCs under a wide variety of not only directional tunings, but also spatial and temporal tunings. Our results confirm

that the DS RGCs encompass multiple unique cell types, provide additional characterization of each type, and highlight the need to study these cells as a population. The development of this analysis pipeline also provides an opportunity to record from transgenic mouse lines that alter the function of specific genes or cell types potentially involved in DS RGC development and tuning.

There are a few caveats that must be addressed. For example, in a single recording, we can confidently identify approximately 400 RGCs over an area of 0.526 mm^2, for a density of ~712 cells/mm^2. This is a much lower density than anatomical studies find, which suggest a density closer to 3300 cells/mm^2 (Jeon et al., 1998). There are several possible explanations: firstly, that the cells could in fact be slightly less dense than in anatomical studies, due to the fact that the retina must be partially squashed against the electrodes in order to make good contact, which could artificially spread the cells. Another explanation may be that certain cell populations are simply not detected on the MEA, either because the spikes are not robust enough to be found on the array, or the cells are not being stimulated enough to have their visual responses adequately characterized. An example of this can be seen when the ON DS cells respond very poorly to the 60 Hz white noise, but respond better to the 30 Hz white noise.

A critical outcome of this study was to determine if we could in fact detect the newly described molecularly marked mouse DS RGCs. Not all cell populations that have been described in literature were found in this study. We did not detect an OFF population moving ventrally (Kim et al., 2008). We should also note that we could

not find more than one distinct population of ON/OFF DS cells that select in the nasal direction (Huberman et al., 2009; Kay et al., 2011a; Rivlin-Etzion et al., 2011). Because we were able to find the receptive field mosaic of ON/OFF DS cells, it seems likely that there was only one population found. This could be due to a shortcoming of the recording method, or it could suggest that the initial distinctions between the genetically labeled lines were incorrect. We also did not find two distinct populations of ON DS cells (Kanjhan and Sivyer, 2010; Hoshi et al., 2011), but as evidenced in the data, the ON populations were more difficult to detect on the MEA than the ON/OFF DS cells. A possible reason for this could be that for a five second window, a cell with a preference for slow-moving stimuli has fewer opportunities to respond than a cell with a preference for fast-moving stimuli.

In our study, we saw that the distribution of angles between RGC populations was not always consistent. This finding hints at the possibility that the "classical" descriptions of DS cell directional preferences may not be adequate descriptions. A computational study of rabbit DS RGCs has shown that having a moderate jitter in the distribution of ON/OFF DS population directions does not strongly affect the efficiency of encoding all four "cardinal" directions. This implies that some of the inconsistency in the population directions could simply be a result of evolutionary cost-effectiveness (Fiscella et al., 2015). A more interesting theory for this result, however has also proposed. In early work with calcium imaging and single unit recording over the entire retina, it has been seen that the DS cells might actually have a more "global" encoding system, selecting for different directions depending on

where in the retina they reside (Sabbah et al., 2015). This may coincide with our finding that recordings from more lateral retina show ON DS cells with a 90°/90°/180° distribution, and recordings from more medial retina show closer to 120°/120°/120° distribution.

In addition to characterizing the DS cells using a typical moving grating stimulus, we also use our previously established white noise analysis to show that functional receptive fields tile for several DS cell types. Beautiful work has shown that anatomical dendrites of DS cells form mosaics (Amthor and Oyster, 1995). It has also been shown in rabbit retina that the receptive fields of DS cells tend to tile the visual space (Devries and Baylor, 1997). Our study is consistent with these previous findings, and lends credence to the idea that each of the subpopulations of DS cells corresponds to a biologically relevant cell type, rather than a mixture of independent cell types that have properties so similar to each other that they can't be distinguished through functional analysis.

Finally, our study shows some subtle distinctions may exist between the ON/OFF type DS cells subpopulations in terms of their speed tuning. In past studies, speed tunings have not been distinguished in more detail than showing that ON DS RGCs prefer slow motion, and ON/OFF DS RGCs prefer fast motion (Oyster et al., 1972; Sivyer et al., 2010). However, several pieces of evidence could suggest that the three ON subtypes and four ON/OFF subtypes are not simply "rotated" versions of two unique RGCs. Firstly, it has been shown that the DSness in mouse RGCs is established before eye opening (Elstrott et al., 2008). Furthermore, much work has

been done to find molecular markers for DS cells, such as transgenic GFP lines, and unique proteins that can isolate DS RGC subtypes via immunostaining (Kay et al., 2011a; Rivlin-Etzion et al., 2011; Dhande et al., 2013). The fact that some DS subtypes have a unique molecular identity could contribute to different ON/OFF DS RGC types having different tuning.

SECTION 3.2: MATCHING FUNCTIONAL CELLS WITH ANATOMICAL CELLS

A major goal in neuroscience is to understand the role of neurons in encoding and transmitting information. To do this, we need to study not only a neuron's data-rich spiking patterns, but also a neuron's physical anatomy, as both function and structure are essential to a working neural circuit. Electrophysiologists have long experienced the problem of a trade-off between low-throughput, anatomically accurate single cell recordings, and high-throughput multi-cellular recordings with poor anatomical correlations. In this study we present a novel technique that combines a large-scale, microelectrode array recording with precise cell identification through optogenetic stimulation and subsequent confocal imaging. Considering the many molecular options available for optogenetic gene expression, this method becomes a versatile tool for matching functional cell types to anatomical cell types.

3.2.1 Matching ChR2-tdTom Labeled RGCs to Functional Responses and Anatomical Images

Introduction

Mammalian retina has long been used as an excellent model system for studying neural circuits. There are many neural subclasses and each of those with many subtypes, from photoreceptors, to the bipolar cells, to retinal ganglion cells (RGCs), which are the output cells of the retina (Masland, 2001). It is highly organized, yet still more accessible than cortical neural circuitry, and as such is an

excellent place to approach one of the fundamental goals of neuroscience: to match neuronal structure to function. The retina provides some of the most elegant examples of neural structure contributing to function, for example, the laminar terminations of RGC dendrites in the inner plexiform layer determine their ability to respond to the onset versus the offset of light, and the width of the dendritic field of RGCs defining their visual receptive field size (Wassle and Boycott, 1991). In particular, the mouse is an excellent model for studying retinal neural circuits, as there are many available genetic tools for probing the system (Huberman and Niell, 2011).

There have been many techniques used to describe the function and structure of retina cells. Single cell patch clamp recordings allow for direct recording from a neuronal cell, then dye filling can elucidate the anatomy, (Schmidt and Kofuji, 2011) but this is a time consuming and laborious effort. Calcium dye imaging has been used to record from large numbers of RGCs simultaneously, and can be combined with dye filling and genetic techniques to associate function with structure (Baden et al., 2016), but this technique is unable to get high-resolution spike timing data. Microelectrode arrays (MEAs) are a compromise between these functional techniques, offering high resolution spike timing data with the ability to record from many cells simultaneously (Litke et al., 2004), however, in this technique assigning the recorded spikes to an individual neuron is not a trivial task, as the ability to locate a cell based on triangulation of the extracellular voltage recordings is not precise enough to identify a cell at the density of RGCs exist in the retina.

One method that has recently been described at addressing this problem relies on matching the electrophysiological image (EI) with anatomical axons labeled with retrogradely infected viral GFP (Li et al., 2015). While this study proved highly successful in matching some anatomical primate RGCs with physiological EIs, the shortcoming of this technique is that it can only match cells with extended axons over the MEA, and relies on successful retrograde labeling of the recorded cells.

Here we describe a novel technique that does not rely on the EI, but rather on the spike waveforms and well-defined soma location using an optogenetic approach. Optogenetics is a powerful technique in neuroscience, making use of a bacterial protein, Channelrhodopsin-2 (ChR2). ChR2 is a light sensitive cation channel membrane protein that allows sodium ions into a cell in response to high-intensity blue light (Nagel et al., 2003). Expression of ChR2 in a neuronal cell has been shown as an elegant and reliable method to elicit spike trains in neuronal cells (Boyden et al., 2005; Deisseroth et al., 2006; Zhang et al., 2006).

In this study, we use an MEA technique to simultaneously record from hundreds of mouse RGCs while determining their functional responses. By expressing ChR fused with a fluorescent protein (in this case, tdTomato, tdTom) in a Cre-dependent fashion (Madisen et al., 2012). Then, using a Cre with a sparse labeling in the RGC layer (Ivanova et al., 2010; Rivlin-Etzion et al., 2011; Zhu et al., 2014) we are able to stimulate a subset of the recorded cells with high-intensity blue light. By matching the spike waveforms from the visual stimulations and the optogenetic stimulations, we can match an anatomical cell to its visual response.

Furthermore, these cells can be re-found in confocal imaging of immunohistochemical stains, with the potential to further associate molecular identities with the functional and anatomical.

Results

In these experiments, we recorded from retinas that were expressing a ChR2-tdTomato fusion protein, both with visual and optogenetic stimulation (Fig 3.13A). Visual responses were first recorded as they were in regular wildtype retinas, using a binary white noise to produce visual STAs (Fig 3.13B), and a shortened moving gratings parameter scan with 8 equally spaced directions, 3 spatial periods (576μm, 1152μm, 2304μm), and 5 temporal periods (0.53 sec, 1.07 sec, 2.13 sec). Importantly, each recording also produced an electrophysiological image (EI) for the cell (Figure 3.13B, final panel). After the application of pharmacological blockers to prevent any light information from transferring from the photoreceptors to the RGCs (see Methods), the ChR2 expressing RGCs were stimulated with a a microLED array capable of stimulating ChR2. This produced an optogenetic STA (optoSTA), as well as an EI (Figure 3.13C).

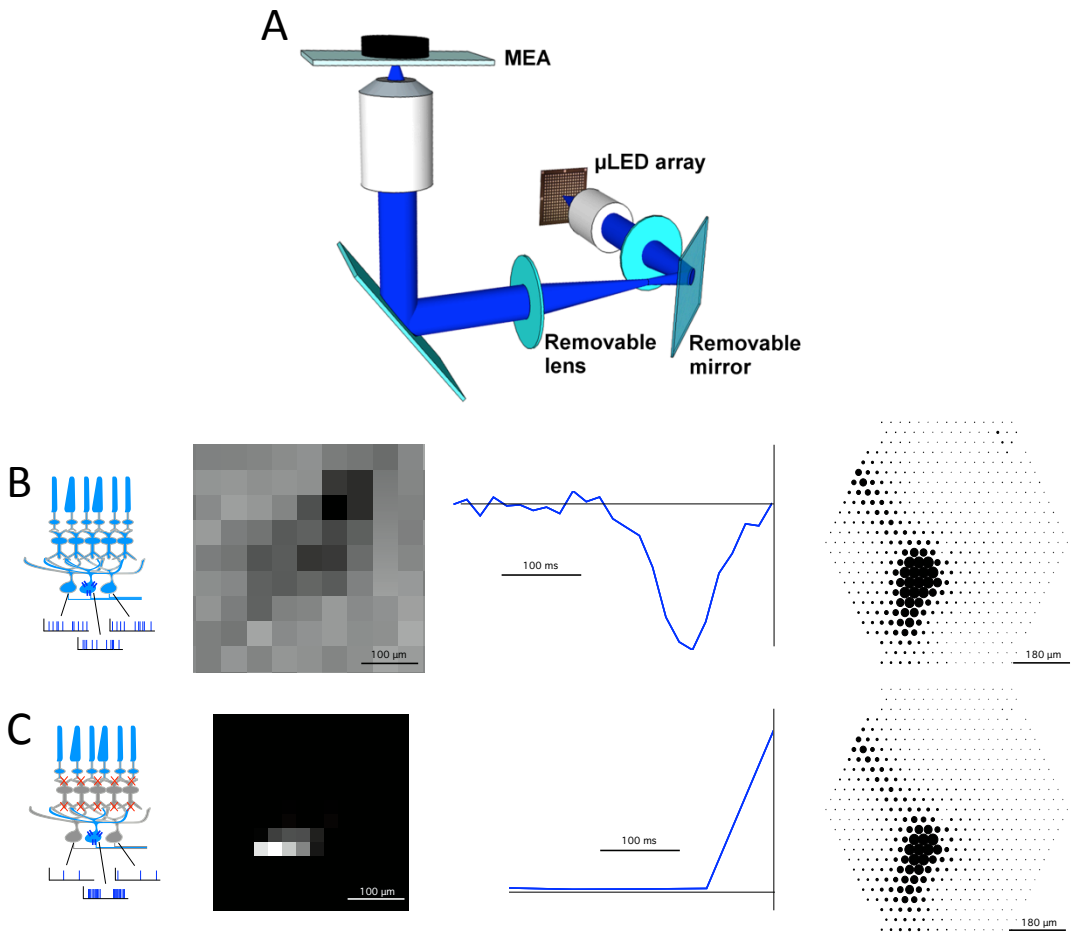

Figure 3.13: Example visual and optogenetic STAs. A) Diagram of recording setup, with both microLED array and CRT monitor able to project to the same preparation via a removable mirror. B) In the visual stimulation recording paradigm, all RGCs receive input from rods and cones, producing visual STAs, TCs, and an EI. C) In the optogenetic stimulation paradigm, all rod and cone input is blocked with pharmacological blockers, so only ChR2 expressing cells respond. These RGCs show optoSTAs (generally smaller than the visually evoked ones, opto TCs, and an EI. If an EI in the visual recording matched an EI in the optogenetic recording, that cell's visual response could be mapped to an anatomical cell.

The optoSTA was matched to the visual-evoked cells based on their EI. However, the optoSTA must also be used to match that cell to an anatomical cell. This is possible because a cell's optoSTA is much more closely correlated to its location than its visual STA, since the optoSTA is generated by light hitting the cell's soma, rather than the photoreceptors that connect through many interneurons to the cell's dendritic tree. Prior to drug application, the transgenic retinas were imaged while still over the MEA (Fig 3.14A). This provided a guide to align the stimulus. The location of the LED array in relation to the MEA and retina was noted before and after each stimulus to ensure that no drift had occurred (Fig 3.14B). This allowed the optoSTAs (Fig 3.14C) to be aligned over the retina on the MEA (Fig 3.14D). After removal of the retina, restaining of tdTomato, and high magnification z-stack confocal imaging, the images were re-aligned over the MEA fluorescent images. The cell body under the optoSTA can now be seen in much better detail (Fig 3.14E). By carefully following the axon of the cell in question, it is manually traced out (Fig 3.14F). We then returned to the functional properties of the cell to look at the EI, formed by the averaging the voltages on each electrode each time the cell spiked. We saw that the axon of the optoSTA cell's EI nicely matched the axon of the labeled cell (Fig 3.14G). As a comparison, we also looked at the EI axon trace of a neighboring RGC that showed no responsiveness to the optogenetic stimulation. This EI did not match the labeled cell's axon (Fig 3.14H). Many optoSTAs were found in each recording (Figure 3.14I).

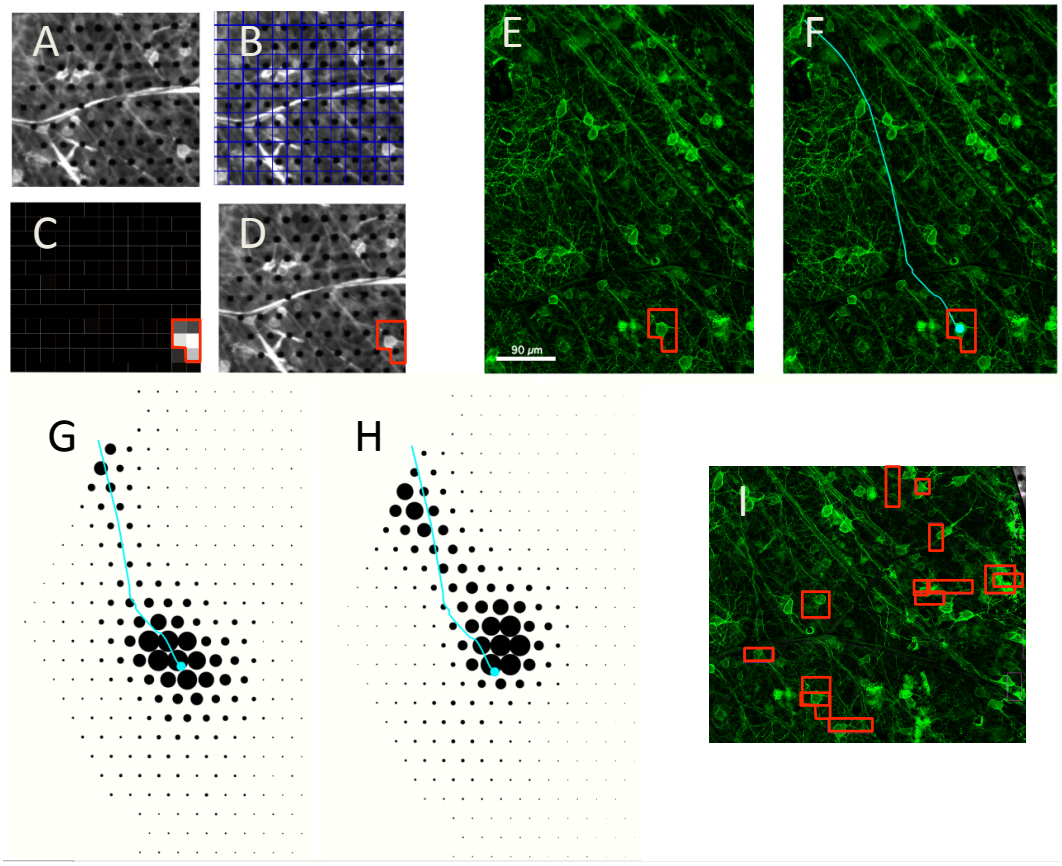

Figure 3.14: Matching anatomical cell with electrophysiological cell. A) Fluorescent image of the retina while still over the MEA. Cells that are fluorescent express ChR2-tdTom. B) Grid representing the LED array used for ChR2 stimulation. C) OptoSTA of a particular cell, with red outline denoting relevant pixels. D) STA red outline placed over the image of the retina on the array. E) After recording, cells were re-stained and imaged on a confocal microscope, then re-aligned over the MEA image. Red outline shows the optoSTA. F) Cyan line shows the axon of the cell body under the red box. G) Cyan line indicating the axon trace in (F), overlaid on the EI of the cell with the optoSTA in (C), showing a very close match. H) A nearby neuron to the neuron in (G) that had no optogenetic response, and had an EI that doesn't closely match the cyan trace. I) Many optoSTAs are found per retina.

Finally, all cells whose functional spikes were successfully matched to the spikes of an anatomical cell were examined. We first took all the cells per retina that had a clear optogenetic response (between 10 and 70, depending on how many cells

were under the array and how many times the array could be moved to a new location). We then mapped visual recordings to the optogenetic recordings, using the similarities between the 182-element neuron finding vectors and the EIs to find the same cells in each recording. We found that approximately 47% (7/15) of optogenetically activated cells with anatomical counterparts could be successfully mapped to cells that were spiking during the visual recording in the Grik4-Cre mouse, and approximately 67% (2/3) of optogenetically activated cells with anatomical counterparts could be successfully mapped to cells spiking during the visual recording in the CRH-Cre mouse (Fig 3.15A). We then looked further at the direction selectivity of optogenetically active cells, and found that in Grik4-Cre mice there was about a 57% (4/7) chance of mapped cells being DS (Fig 3.15A,B), while no cells in the CRH-Cre mice were both optogenetically sensitive and DS (Fig 3.15A,C).

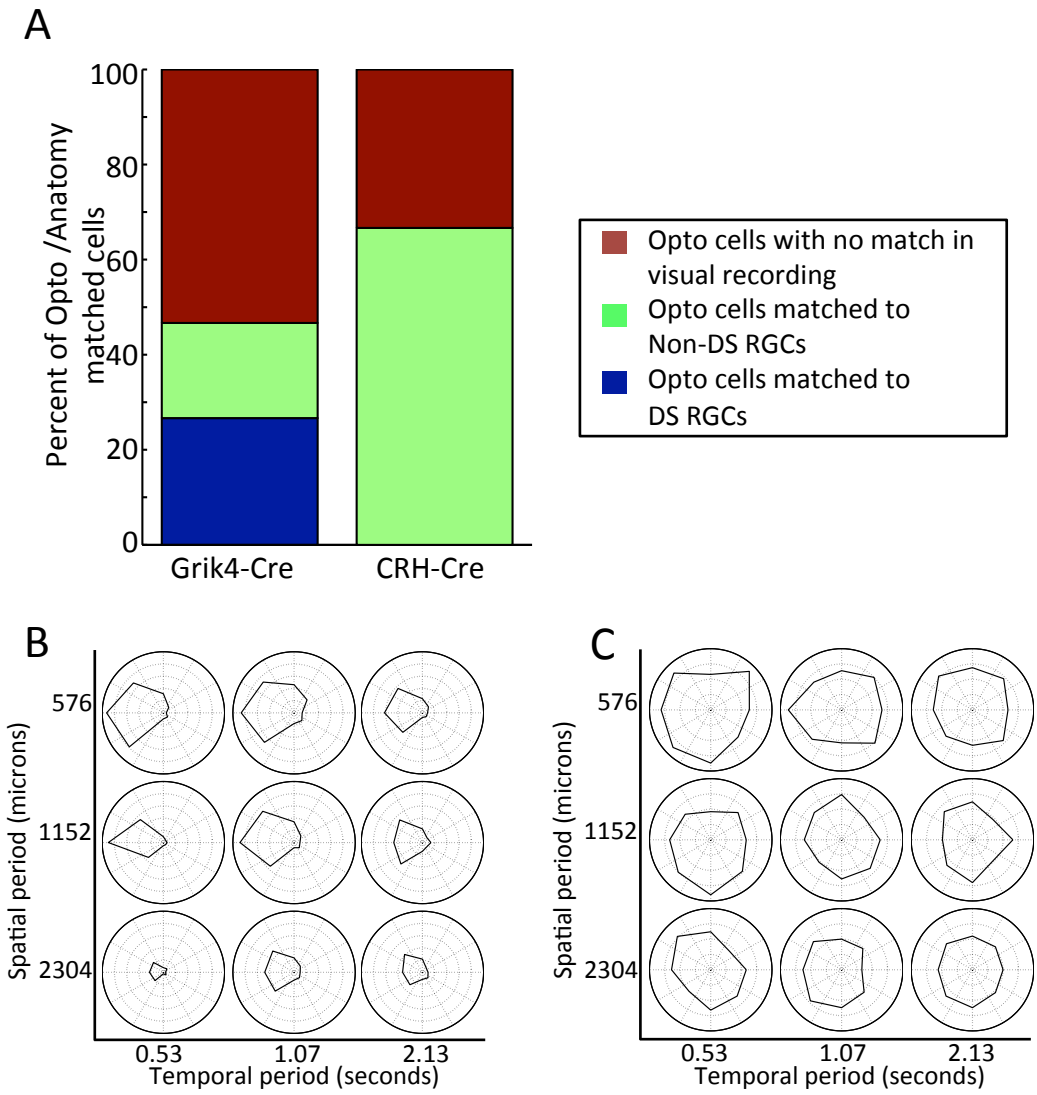

Figure 3.15: Comparison of DS responses of Grik4-Cre and CRH-Cre expressing cells. A) For one Grik4-Cre recording, and on CRH-Cre recording, the total number of cells with an optogenetic response was considered to be 100%. We saw that comparing the two preparations, 47% and 67% of optogenetically stimulated cells had matching counterparts in a visual recording. In the Grik4-Cre recording, approximately 27% of those cells were DS, and in CRH-Cre recording, none of those cells were DS. B) Example of ChR2-expressing DS cell in Grik4-Cre recording. C) Example ChR2-expressing non-DS cell in CRH-Cre recording.

Discussion

We have here described a method to associate high throughput electrophysiological data with anatomical cells using an MEA recording system and transgenically expressed ChR2-tdTomato in the retina. We have shown that a spatial-temporal optogenetic stimulus can be analyzed much in the same way a spatial-temporal visual stimulus is, effectively confirming that ChR2 can turn any array of neurons into a kind of "retina". This could potentially be adapted to other acute or cultured preparations, such as slices from cortex or hippocampus, which might benefit from the ability to match a subset of cells to their functional response on the MEA (Ito et al., 2014).

We showed that when a cell with a clearly labeled axon had an optoSTA over the cell's soma, that axon matches nicely to the cells' EI. Indeed, matching fluorescently labeled axons to EI axon traces is a previously verified technique for matching functional cells to anatomical cells on an MEA (Li et al., 2015). The advantage of our technique is that we don't need to use axons, as the optoSTA can be mapped to just the cell soma. In this way, our technique provides more flexibility, in that it can identify cells that have poorly labeled axons, axons that are ambiguous, or cells on the edge of the MEA that have axons traveling away from the MEA center.

Even though only a fraction of the cells are optogenetically active and thus can be matched, the MEA system provides a population level context in which that cell exists. In our experiment, we saw that a fraction of Grik4-Cre expressing RGCs were DS responsive. This corresponds to the previously known result that ~30% of

Grik4-Cre mice respond to nasal selecting RGCs (Rivlin-Etzion et al., 2011). Conversely, none of the CRH-Cre expressing RGCs had a DS response, which is consistent with the fact that CRH-Cre generally expresses in displaced amacrine cells and mono-stratified RGCs (Zhu et al., 2014).

This technique provides the ability to match functional cells to anatomical cells on the MEA system limited only by the possible expression patterns of ChR2. In our experiments, we used a Cre-dependent ChR2-tdTomato fusion protein at the Rosa26 locus, combined with two different Cre lines. This reporter could also be combined with virally expressed Cre recombinase for random and sparse labeling (Ahmed et al., 2004) or the recently described Cre-DOG system that allows Cre to be expressed with expression of transgenic GFP lines (Tang et al., 2015). If the density of cells is too high to accurately get anatomical data, this method can also utilize a sparser labeling technique using a viral reporter (Zhu et al., 2014). Our method can take full advantage of the vast availability of mouse genetic toolboxes.

SECTION 3.3: GENETIC MUTANT ANALYSIS

The advances I've made in characterizing wildtype mouse retinas can be applied to the study of developmental mechanisms through genetic manipulations. By running functional analysis the retinas of mice that are deficient in genes important for axon guidance or retinal development, and comparing these to wildtype and littermate controls, I can begin to discern the roles these genes play in establishing and maintaining retinal circuitry. Note that both of these projects were collaborations that involved closer examinations of genetic and anatomical phenotypes of the mutants, but my focus was primarily on the functional phenotypes.

3.3.1: DSCAM analysis

Introduction

DSCAM is a cell adhesion molecule found to be expressed in the retina (Fuerst et al., 2010). It is needed for self avoidance and mosaic spacing of the RGC dendrites (Fuerst et al., 2008, 2009). In DSCAM$^{2j/2j}$ mutant mice (hereafter referred to as DSCAM$^{-/-}$), the regular spacing of cell somas of dopaminergic, bNOS positive, cholinergic amacrine cells, and all tested RGC types is disrupted. In addition, the dendrites of these neurons tend to fasciculate, resulting in uneven coverage of the retina (Fuerst et al., 2009, 2010). Electroretinogram responses in DSCAM$^{-/-}$ retinas indicate that light responsiveness and functional synapses are maintained (Fuerst et al., 2009). In this study, we aimed to determine how the anatomical abnormalities in the retina affect functional response properties of distinct retinal pathways by

comparing the RGC responses to visual stimulation between wildtype and DSCAM$^{-/-}$ retinas. Using a large-scale multielectrode array (MEA) to record the extracellular electrical activity from hundreds of RGCs simultaneously, we find that DSCAM is required for the formation of direction selective circuits. Loss of DSCAM resulted in fewer DS cells than wildtype, and of those DS cells, they had a weaker response.

Results

Direction selective RGCs require inputs from amacrine cells to form their selectivity; therefore, these circuits may be more disrupted than those of the ON or OFF RGCs. DS RGCs were identified based on the responses to gratings moving in different directions. We identified four wildtype DS RGC types with four approximately orthogonal preferred directions (Oyster and Barlow 1967) (Fig 3.16A), consistent with them being ON/OFF DS RGCs. However, since responses to our stimulus did not distinguish ON vs ON/OFF DS RGCs, it is possible that some of the selected cells are ON DS RGCs. We found that the fraction of DS RGCs among the detected RGCs was, on average, 10 times lower in the DSCAM$^{-/-}$ retinas than in the wildtype or DSCAM$^{+/-}$ retinas ($p = 1.2x10^{-3}$, two-sided Kolmogorov–Smirnov test) (Fig 3.16B, C). Furthermore, we found that the few DSRGCs that we could identify in DSCAM$^{-/-}$ retinas had a lower direction selectivity ($p = 2.4x10^{-7}$, t-test; Fig 3.16D) and broader tuning curve ($p = 5.7x10^{-4}$, t-test; Fig 3.16A, B, E) than those measured in wildtype retinas.

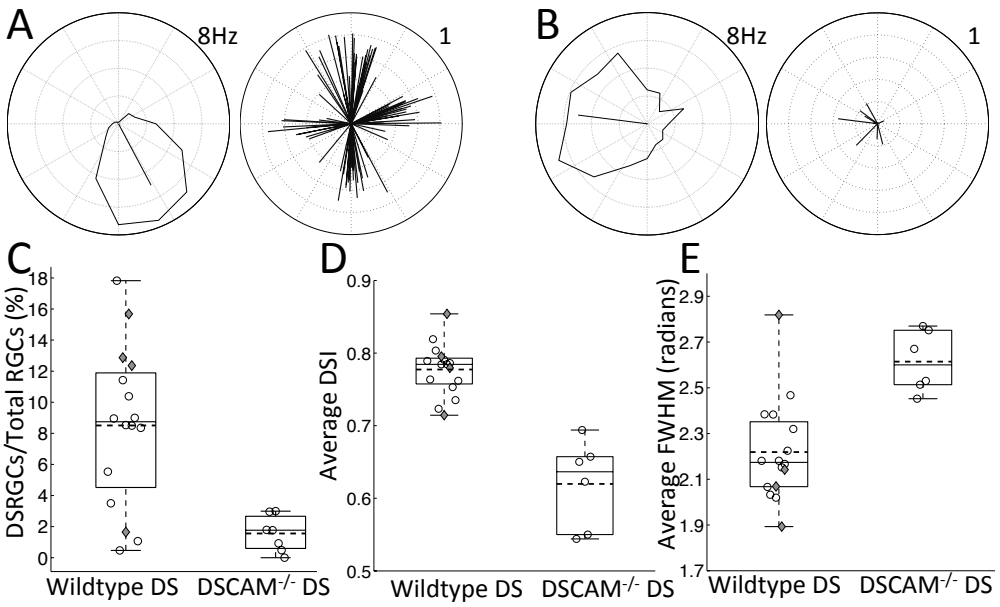

Figure 3.16: DSCAM$^{-/-}$ retinas have fewer and weaker DS RGCs. (A and B) The left polar plots show the tuning curve of the spike rate (spikes/sec) of a single DS RGC. Normalized spike rates were vector summed to produce a Direction Selective vector for each neuron. The right polar plots show the Direction Selective vectors for all DS RGCs in one wildtype retina A) and one DSCAM$^{-/-}$ retina B). C) Box plot showing the percentage of RGCs that are DS RGCs for each retina. ($p = 1.2x10^{-3}$, Kolmogorov–Smirnov test) D) Box plot showing the average DSIs for DS RGCs in wild-type and DSCAM$^{-/-}$. ($p = 2.4x10^{-7}$, t-test). E) Box plot showing the average full width at half maximums (FWHMs) for DS RGCs in wild-type and DSCAM$^{-/-}$. ($p = 5.7x10^{-4}$, t-test). For all box plots, points indicate individual retinas, with circles indicating mutant or wild-type, and grey diamonds indicate DSCAM$^{+/-}$. The center line indicates the median, the dotted line indicates the average, the box edges indicate the 25th and 75th percentiles, and the whiskers indicate the most extreme datapoints. DSCAM retinas with no identified DS cells are not included in the DSI and FWHM plots. Note box plots do not necessarily start from zero. **p<0.01, ***p<0.001.

Discussion

Direction selective circuitry is severely compromised in DSCAM mutant retinas. DSCAM$^{-/-}$ retinas had far fewer DS RGCs than wildtype, and those that were identified as DSRGCs had weaker direction selectivity. The retinal circuitry that creates DS responses is more complex than that of non-DS circuits, and some DS circuits rely on the asymmetric synapse formation of starburst amacrine cells with DS RGCs (Trenholm et al., 2011). Due to massive RGC dendritic fasciculation in the absence of DSCAM, ON/OFF DS RGCs may not be able to connect to the starburst amacrine cells in a spatial manner that properly establishes preferred and null directions. Consistent with this, the stratification of ChAT immunoreactivity in the inner plexiform layer, which represent the processes of starburst amacrine cells, are disrupted in the DSCAM$^{-/-}$ retina (Fuerst et al., 2010; Schramm et al., 2012). Because starburst amacrine cells do not express DSCAM, the defect in the organization of ChAT-positive processes in the DSCAM$^{-/-}$ retina is likely a secondary effect of the processes of these cells branching to locate synaptic sites on the highly fasciculated dendrites of the RGCs. This would lead to both lamination defects and improper establishment of connections with ON/OFF DS RGCs. An alternative explanation of the scarcity of the direction selective responses in the DSCAM$^{-/-}$ retina could be that the DS RGCs have undergone cell death. We observe more CART positive cells in the DSCAM$^{-/-}$ retinas compared to wildtype, which indicates that the DS RGCs have not undergone cell death. It has been previously reported that the lack of DSCAM

results in defects in developmental cell death, which explains the increase in CART positive RGCs counted in the DSCAM$^{-/-}$ retinas (Fuerst et al., 2010).

3.3.2: Satb1/2 Analysis

Introduction

Satb1 and Satb2 (special AT-rich sequence binding protein 1 and 2) are related transcription factors (Nakagomi et al., 1994; FitzPatrick et al., 2003). It has been shown that Satb1 plays a role in maintaining the density of cortical neural dendritic spines (Balamotis et al., 2012). It has also been shown that Satb2 is involved in cortical neuronal development and fate determination (Britanova et al., 2008; McKenna et al., 2015). Satb2 is expressed in the retina in a subset of amacrine cells and RGCs (Kay et al., 2011b). Previous studies in our lab showed that Satb1 and Satb2 co-express with several known DS RGC transgenic markers (Sweeney, unpublished data). Satb1 and Satb2 co-express with DRD4-GFP and TRHR-GFP mouse lines, which both label nasal selecting ON/OFF DS RGCs (Huberman et al., 2009; Rivlin-Etzion et al., 2011) and Satb1 co-expresses with the HB9-GFP mouse line, which labels ventrally selecting ON/OFF DS cells (Trenholm et al., 2011) (Sweeney, unpublished data). We examine Satb1 and Satb2 double knockout mice (hereafter referred to as Satb1/2$^{-/-}$) in the context of functional DS cells, using the previously described DS parameter scan analysis to distinguish the different types of DS cells. We find that while ON DS cells are unaffected by the loss of Satb1 and

Satb2, the ON/OFF DS cells show a significant decrease in the Satb1/2$^{-/-}$ retinas. Furthermore, the decrease in ON/OFF DS cells seems to be non-uniform over the different ON/OFF subtypes, with the nasal selecting group showing the greatest lost, and the ventral selecting group showing the least loss.

Results

Breeding Satb1-floxed (Balamotis et al., 2012) and Satb2-floxed (Srinivasan et al., 2012) mice to a Pax6-Cre mouse (Okawa et al., 2014) produced double knockout mice with mutant regions only in the far peripheral nasal and temporal retina. During dissection, retinas were carefully dissected and arranged to place a mutant area over the array. The spiking activity of RGCs within these retinal areas was recorded in-vitro on a planar 512-electrode array. DS RGCs were identified based on their responses to a full field drifting gratings of various direction and spatial and temporal periods. DS RGCs were classified into ON and ON/OFF types using their spatio-temporal tuning. During the recording, PNA stain was applied to provide landmarks for the retina on the array (Fig 3.17A,C). After recording, the retinas were immunostained to ensure that the recorded area was Cre positive and either displayed Satb2 expression if it was a littermate control recording (Fig 3.17B) or lacked Satb1/2 expression if it was a Satb1/2$^{-/-}$ recording (Fig 3.17D).

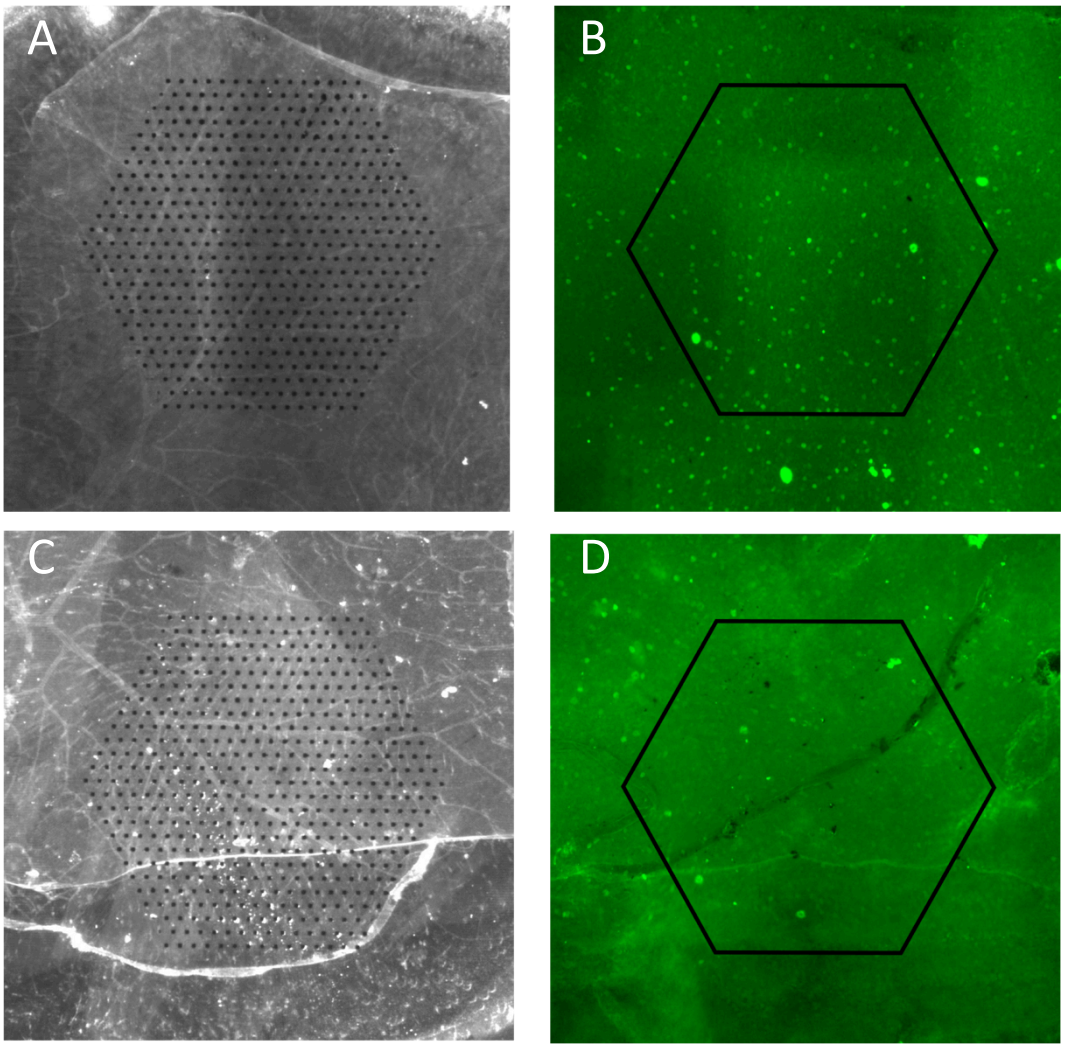

Figure 3.17: Satb1 and Satb2 confirmed to be absent in knockout recordings. A) Littermate control (LMC) retina over the array, stained with PNA during recording. B) Same LMC retina showing Satb2 expression, hexagon shows array location after re-alignment. C) Knockout (KO) retina over the array, stained with PNA during recording. D) Same KO retina showing Satb2 expression, hexagon shows array location after re-alignment.

After confirming that the areas recorded from were either positive or negative for Satb2, we analyzed the functional responses of Satb1/2 double knockout mice for possible defects in direction selectivity. Using the multi-parameter drifting gratings

stimulus and analysis described in Section 3.1.2, we were able to consistently tease out 7 distinct populations of DS cells. We saw that there was a significant reduction in ON/OFF DS cells in the mutant mice compared to littermate controls (LMC) ($p = 0.01$ t-test, Fig 3.18A). Conversely, we found that the number of the detected ON DS cells was unchanged between the KO and LMC animals ($p = 0.50$, t-test; Fig 3.18B). We then broke the DS cell populations down by directional preferences. We saw that the nasal selecting population of ON/OFF DS cells was significantly reduced ($p = 0.002$ t-test; Fig 3.18C), while the other ON/OFF DS populations as well as the ON DS populations were not significantly affected.

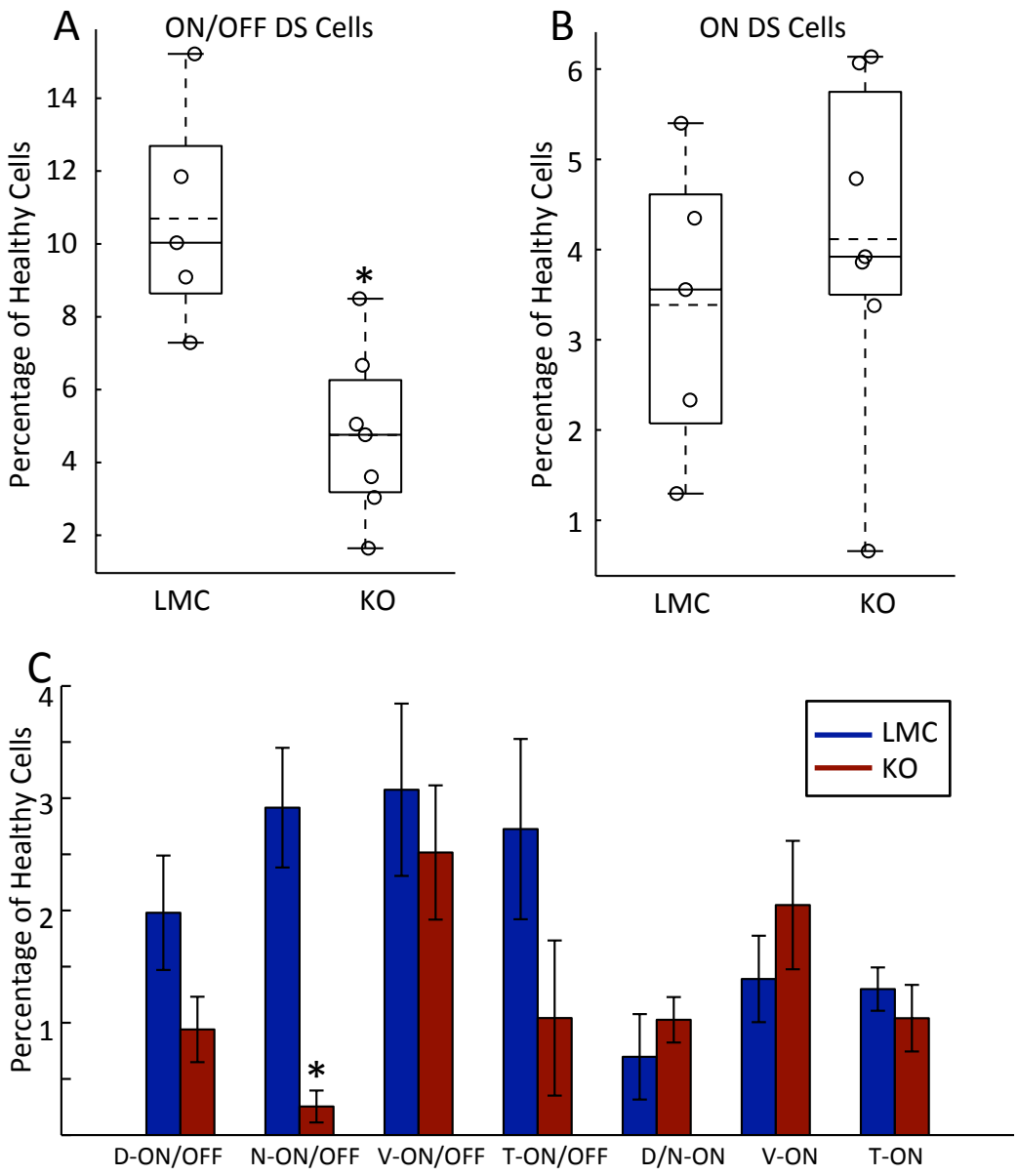

Figure 3.18: Satb1 and Satb2 differentially affect DS RGC subpopulations. A) The overall number of ON/OFF DS cells is reduced in Satb1/2 KO retinas. (LMC mean = 10.7%, KO mean = 4.8%, t-test, p = 0.01). B) The number of ON DS cells remains unaffected (LMC mean = 3.4%, KO mean = 4.1%, t-test, p = 0.50) For A) and B), solid line represents medians, dotted line represents mean, the boxes represent 25th and 75th quartile, whiskers represents extent of data set. C) Deletion of Satb1/2 selectively decreases the number of nasal selecting ON/OFF DS cells (t-test, p = 0.002).

Discussion

We have shown that Satb1, Satb2, or both transcription factors are required for the correct development of direction selective pathways in the retina. In particular, we show that the different DS pathways are affected differently, with the ON DS cell populations having no dependence on the presence of these transcription factors, and the nasal selecting ON/OFF DS cells being functionally lost in the Satb1/2$^{-/-}$ retinas. Further studies are needed to determine the individual roles of the two transcription factors and to test if they play a role in the survival, maintenance or wiring of the DS RGCs.

It has been shown that Satb1 and Satb2 co-express with CART staining, as well as express in several of the GFP labeled mouse lines, specifically DRD4-GFP, TRHR-GFP, and Satb1 only is expressed in HB9-GFP (Sweeney, unpublished data). There is also preliminary work that shows that Satb2 at least is not expressed in the Hoxd10 mouse line, which labels ON DS cells and temporal ON/OFF DS cells (Huberman, unpublished data). These molecular studies generally corroborate with the functional results. Satb1/2 is expressed in nasal selecting ON/OFF DS cells, and that population is lost in the Satb1/2$^{-/-}$ retinas. Satb1/2 is not expressed in ON DS cells or temporally selecting ON/OFF DS cells, and those populations are not affected by the double knockout. Of interest is the result for the ventrally selecting ON/OFF DS cells, as Satb1 is expressed in those cells, but the functional ventral ON/OFF DS population was very robust. It could be that for that population, Satb1 plays a different role that is nonessential to the cell's functional identity.

Finally, as these experiments were highly preliminary, they had the odd feature of being done on the double knockouts. The reasoning for this is that because Satb1 and Satb2 are so closely related, it is possible that they could have redundant functioning in the retina, so the double knockout might show a phenotype where a single knockout of either might not. Conversely, studies in embryonic stem cells suggest that Satb1 and Satb2 can counteract each other with regard to the cell either remaining pluripotent or differentiating (Savarese et al., 2009). In either case, it will be important in future experiments to test the single knockouts of Satb1 and Satb2 to determine if only one of the genes is essential for the functional identity of nasally selecting ON/OFF DS RGCs.

CHAPTER 4: CONCLUSIONS AND FUTURE WORK

In this chapter I reiterate the conclusions of my thesis projects, give an example of a future direction that can be taken using this work as a basis, and finally remark on the broader implications of my work.

Overview of Research Presented

Over the course of my thesis, I have made several advances in our ability to functionally detect RGCs using the MEA system, associate MEA functional data to anatomically defined cells, and put these analyses to use in genetic studies.

In my first major goal, I present two projects in which I improve our ability to functionally classify mouse RGCs. Using a white noise and full field flash stimulus, I show that five distinct cell types, three OFF and two ON, can be detected on the MEA consistently. Moreover, they can be successfully mapped to cell types found in other similar retinal preparations. Variation between preparations was a clear influence in preventing straightforward associations from retina to retina, and care should be taken in future classification studies.

I also showed that using a multiparameter drifting sine wave stimulus, I could characterize DS cells not only in terms of their preferred direction, but also in terms of their preferred speed and width. This showed some known differences as a control, such as the difference in speed preference between ON and ON/OFF DS cells. The extensive stimulation parameter space also allowed me to examine the tuning parameters of DS RGCs in finer detail, and revealed some as of yet undescribed

differences in spatial/temporal preferences between the different populations of ON/OFF DS cells.

My second major goal was to match anatomy to physiology in the MEA recording paradigm. This addresses a major shortcoming of this technique, namely that recordings done on the MEA have no straightforward correspondence to the physical cell producing the detected voltages. To accomplish this, I used a mouse reporter line that expressed ChR2-tdTom when crossed to a Cre line. I showed that the same RGCs could be found from optogenetic stimulation and visual stimulation. Furthermore, optogenetic STA frequently corresponded closely to the location of a fluorescent cell, and when axons were visible, the axon of the labeled cell matched with the EI of the optogenetically stimulated cell. Finally, I showed that there was a detectable difference in the RGC populations of different Cre expressing mouse lines.

My third major goal was to take some of my previously accomplished analysis strategies and apply them to an experimental paradigm. To this end, I concentrated on my work with detecting and identifying DS cells. I first looked in the DSCAM knockout mouse, which is missing a cell adhesion molecule with a known expression pattern in the retina. My simple single parameter DS analysis protocol reveled that DSCAM mice have far fewer DS responding cells. Furthermore, of those RGCs that are DS, they tend to have a lower DSI, which means that the ratio of response in the preferred direction versus the null direction is lower, and they also had on average a larger full width at half height, meaning that the cells were not tuned as sharply for their preferred direction. We propose that this could be a consequence of the DS

RGCs being unable to correctly synapse with the starburst amacrine cells known to facilitate DS responses.

In the second of these projects, I examined the role of two related transcription factors, Satb1 and Satb2, in producing the DS RGC response. Using a more robust version of DS response inducing stimuli, I tested for these transcription factors playing a differential role in the development of different DS cell populations. I found that Satb1 and Satb2 are not necessary for the ON DS response in any of the detectable ON DS cell populations. In the ON/OFF DS populations, however, I saw that Satb1 and Satb2 seem to selectively affect the nasal selecting ON/OFF DS cells, producing a reduced population of only this subtype. This corroborated with molecular evidence showing that Sab1 and Satb2 both co-express with transgenically labeled nasal selecting ON/OFF DS cells.

Future Direction: UV Stimulation

One exciting direction this research can take involves the study of color vision. All the research I have presented involves mono-color visual stimuli on the CRT monitor. However, different photoreceptors express different light sensitive molecules, or opsins, which have similar absorption curves but differ in their peak absorption wavelength (Govardovskii et al., 2000). In particular, mice photoreceptors express either an S-opsin or M-opsin in a region-specific way. Most cones are considered "co-expressing" cones, which express M-opsin and S-opsin, however, in the dorsal retina they express primarily M-opsin, and express a gradient of increasing

S-opsin as measurements move ventrally down the retina (Haverkamp et al., 2005). Additionally, there is a population of "genuine" S-cones, which are sparsely spaced throughout the retina (Haverkamp et al., 2005) (Fig 4.1A).

In our normal stimulation setup, the blue phosphor of the CRT is unable to adequately stimulate the S-cones of the mouse, as the absorption peak of the mouse cone is approximately 360nm (Jacobs et al., 1991) and the blue CRT phosphor emits at approximately 450nm (Fig 4.1B). Using a custom UV projector system, it is possible to isolate S-opsin responses in mouse retina (Wang et al., 2011).

It has been shown that primate RGC response can be broken up by cone color input (Field et al., 2010). I propose a similar study adapted for the mouse retina, in which a very high resolution modified white noise is used. In this stimulus, the color values of the pixels (in this case, either green or UV) also vary independently in a binary fashion, such that per frame, any pixel can be either green, UV, black (both colors off) or cyan (both colors on) (Fig 4.1C). These experiments should be able to parse out the different types of cone contributions to different classes of RGCs, taking advantage of our high throughput recording technique to characterize mouse RGCs at a functional resolution that has never been achieved before.

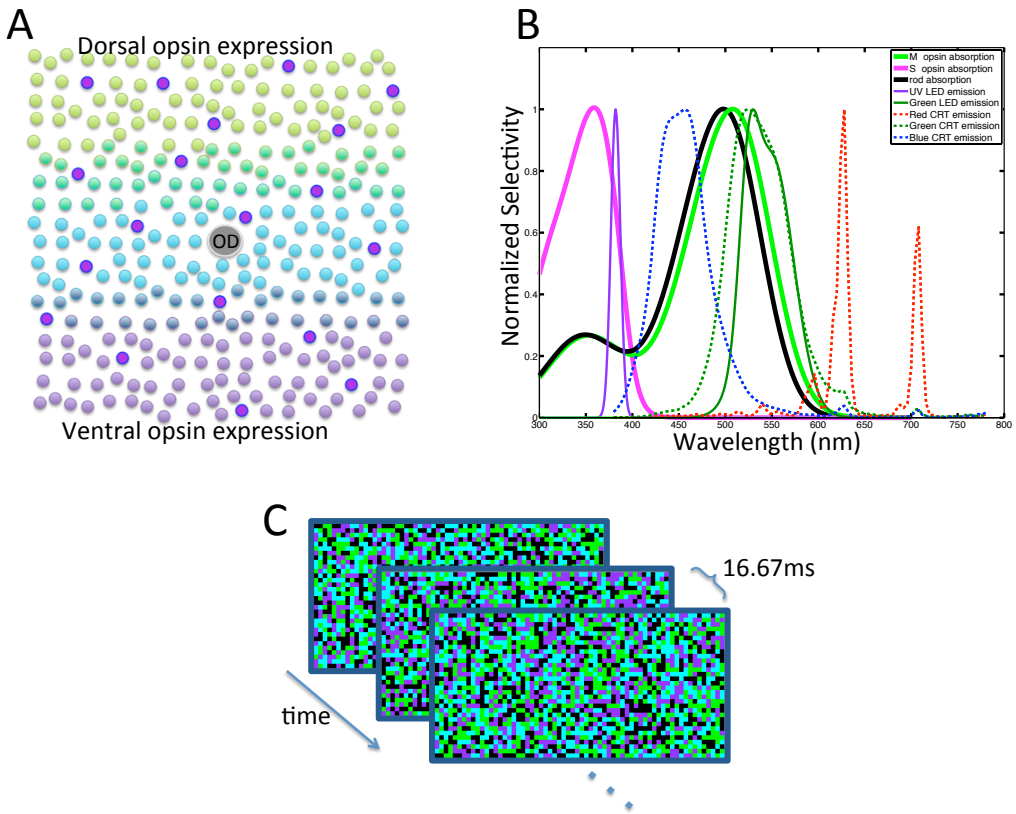

Figure 4.1: Color stimulation of mouse retina. A) In the mouse retina, cone opsin expression consists of "co-expressing cones", which express M-opsin and and increasing gradient of S-opsin in a dorsal-ventral pattern (pastel dots) and also "genuine S-cones" which express S-opsin exclusively and are spread throughout the retina (bright purple dots) Adapted from (Wang et al, 2011). OD stands for optic disk, location of the optic nerve. B) Plotting mouse opsin absorbance spectra and various light source emission spectra together shows that while the CRT cannot effectively stimulate mouse S-opsin, a UV LED can. Formula for absorption curve from (Govardovskii et al, 2000). C) A proposed UV-G white noise stimulus, in which the color value of each pixel follows a Bernoulli distribution with p = 0.5, creating frames of independently colored squares of green, purple, cyan (green + purple), or black (neither green nor purple).

Final Remarks

The work presented in my thesis makes major improvements to our ability to detect and classify functional mouse RGCs. One thing that becomes clear throughout my projects is that in many cases, the ability to distinguish functional types is only as good as our ability to implement and analyze the right stimuli. This was apparent in the DS parameter scan analysis, where a 60 Hz white noise couldn't stimulate an ON DS cell, but a 30 Hz white noise could. This could also be seen by contrasting the DSCAM mutant analysis with the Satb1/2 mutant analysis; while the DSCAM project could only detect the presence or absence of DS cells, the Satb1/2 project could parse out which subtypes of DS RGCs were differentially affected. The more sophisticated stimulus is better able to distinguish subpopulations of cells, and thus can detect a subtler phenotype. I believe that utilizing UV stimulation will have a similar effect, in which new RGC properties will be detected and thus available for scientific inquiry. More broadly, the analyses I developed will be available for future studies in transgenic mice, mutant mice, or more complex animal models.

Neuroscience is a hugely popular and booming field of study. Our drive to understand how we process our perceptions and experiences fires the imagination and is a uniquely human endeavor. Although deciphering the human brain is a daunting challenge, there is much to learn in simpler model systems about the fundamentals of neural coding. At the heart of neural codes is the neuron, a highly diverse type of cell that can take thousands of inputs, integrate them, and produce a relevant output. An elegant example of this is the mammalian retina, which takes light as its input, and

through a series of neural synapses, converts this information into parallel streams of data that enter the brain via the optic nerve. Using the MEA recording system, we can manipulate the input and record the output to hundreds of RGCs simultaneously, giving insight not only into the visual system, but also into the capabilities of neurons in general.

REFERENCES

Ahmed BY, Chakravarthy S, Eggers R, Hermens WT, Zhang JY, Niclou SP, Levelt C, Sablitzky F, Anderson PN, Lieberman A, Verhaagen J (2004) Efficient delivery of Cre-recombinase to neurons in vivo and stable transduction of neurons using adeno-associated and lentiviral vectors. BMC Neurosci 5:4.

Amthor FR, Oyster CW (1995) Spatial organization of retinal information about the direction of image motion. Proc Natl Acad Sci U S A 92:4002–4005.

Anishchenko A, Greschner M, Elstrott J, Sher A, Litke AM, Feller MB, Chichilnisky EJ (2010) Receptive Field Mosaics of Retinal Ganglion Cells Are Established Without Visual Experience. J Neurophysiol 103:1856–1864.

Badea TC, Nathans J (2011) Morphologies of mouse retinal ganglion cells expressing transcription factors Brn3a, Brn3b, and Brn3c: Analysis of wild type and mutant cells using genetically-directed sparse labeling. Vision Res 51:269–279.

Baden T, Berens P, Franke K, Román Rosón M, Bethge M, Euler T (2016) The functional diversity of retinal ganglion cells in the mouse. Nature 529:345–350.

Balamotis MA, Tamberg N, Woo YJ, Li J, Davy B, Kohwi-Shigematsu T, Kohwi Y (2012) Satb1 Ablation Alters Temporal Expression of Immediate Early Genes and Reduces Dendritic Spine Density during Postnatal Brain Development. Mol Cell Biol 32:333–347.

Barlow HB, Hill RM (1963) Selective Sensitivity to Direction of Movement in Ganglion Cells of the Rabbit Retina. Science 139:412–412.

Barlow HB, Hill RM, Levick WR (1964) Retinal ganglion cells responding selectively to direction and speed of image motion in the rabbit. J Physiol 173:377–407.

Berson DM, Dunn FA, Takao M (2002) Phototransduction by Retinal Ganglion Cells That Set the Circadian Clock. Science 295:1070–1073.

Bleckert A, Schwartz GW, Turner MH, Rieke F, Wong ROL (2014) Visual Space Is Represented by Nonmatching Topographies of Distinct Mouse Retinal Ganglion Cell Types. Curr Biol 24:310–315.

Borghuis BG, Looger LL, Tomita S, Demb JB (2014) Kainate Receptors Mediate Signaling in Both Transient and Sustained OFF Bipolar Cell Pathways in Mouse Retina. J Neurosci 34:6128–6139.

Boycott BB, Wässle H (1974) The morphological types of ganglion cells of the domestic cat's retina. J Physiol 240:397–419.

Boyden ES, Zhang F, Bamberg E, Nagel G, Deisseroth K (2005) Millisecond-timescale, genetically targeted optical control of neural activity. Nat Neurosci 8:1263–1268.

Brandstätter JH, Koulen P, Wässle H (1998) Diversity of glutamate receptors in the mammalian retina. Vision Res 38:1385–1397.

Britanova O, de Juan Romero C, Cheung A, Kwan KY, Schwark M, Gyorgy A, Vogel T, Akopov S, Mitkovski M, Agoston D, Šestan N, Molnár Z, Tarabykin V (2008) Satb2 Is a Postmitotic Determinant for Upper-Layer Neuron Specification in the Neocortex. Neuron 57:378–392.

Carcieri SM, Jacobs AL, Nirenberg S (2003) Classification of Retinal Ganglion Cells: A Statistical Approach. J Neurophysiol 90:1704–1713.

Chichilnisky EJ (2001) A simple white noise analysis of neuronal light responses. Netw Bristol Engl 12:199–213.

Chichilnisky EJ, Kalmar RS (2002) Functional Asymmetries in ON and OFF Ganglion Cells of Primate Retina. J Neurosci 22:2737–2747.

Coombs J, van der List D, Wang G-Y, Chalupa LM (2006) Morphological properties of mouse retinal ganglion cells. Neuroscience 140:123–136.

Cruz-Martín A, El-Danaf RN, Osakada F, Sriram B, Dhande OS, Nguyen PL, Callaway EM, Ghosh A, Huberman AD (2014) A dedicated circuit links direction-selective retinal ganglion cells to the primary visual cortex. Nature advance online publication Available at: http://www.nature.com/nature/journal/vaop/ncurrent/full/nature12989.html [Accessed March 26, 2014].

Dacey DM (1993) The mosaic of midget ganglion cells in the human retina. J Neurosci 13:5334–5355.

Deisseroth K, Feng G, Majewska AK, Miesenböck G, Ting A, Schnitzer MJ (2006) Next-Generation Optical Technologies for Illuminating Genetically Targeted Brain Circuits. J Neurosci 26:10380–10386.

Devries SH, Baylor DA (1997) Mosaic Arrangement of Ganglion Cell Receptive Fields in Rabbit Retina. J Neurophysiol 78:2048–2060.

Dhande OS, Estevez ME, Quattrochi LE, El-Danaf RN, Nguyen PL, Berson DM, Huberman AD (2013) Genetic Dissection of Retinal Inputs to Brainstem Nuclei Controlling Image Stabilization. J Neurosci 33:17797–17813.

Dhande OS, Stafford BK, Lim J-HA, Huberman AD (2015) Contributions of Retinal Ganglion Cells to Subcortical Visual Processing and Behaviors. Annu Rev Vis Sci 1:291–328.

Doi M, Uji Y, Yamamura H (1995) Morphological classification of retinal ganglion cells in mice. J Comp Neurol 356:368–386.

Ebrey T, Koutalos Y (2001) Vertebrate Photoreceptors. Prog Retin Eye Res 20:49–94.

Elstrott J, Anishchenko A, Greschner M, Sher A, Litke AM, Chichilnisky EJ, Feller MB (2008) Direction Selectivity in the Retina Is Established Independent of Visual Experience and Cholinergic Retinal Waves. Neuron 58:499–506.

Euler T, Haverkamp S, Schubert T, Baden T (2014) Retinal bipolar cells: elementary building blocks of vision. Nat Rev Neurosci 15:507–519.

Farrow K, Masland RH (2011) Physiological clustering of visual channels in the mouse retina. J Neurophysiol 105:1516–1530.

Field GD, Chichilnisky EJ (2007) Information Processing in the Primate Retina: Circuitry and Coding. Annu Rev Neurosci 30:1–30.

Field GD, Gauthier JL, Sher A, Greschner M, Machado TA, Jepson LH, Shlens J, Gunning DE, Mathieson K, Dabrowski W, Paninski L, Litke AM, Chichilnisky EJ (2010) Functional connectivity in the retina at the resolution of photoreceptors. Nature 467:673–677.

Field GD, Sher A, Gauthier JL, Greschner M, Shlens J, Litke AM, Chichilnisky EJ (2007) Spatial Properties and Functional Organization of Small Bistratified Ganglion Cells in Primate Retina. J Neurosci 27:13261–13272.

Fiscella M, Franke F, Farrow K, Müller J, Roska B, Silveira RA da, Hierlemann A (2015) Visual coding with a population of direction-selective neurons. J Neurophysiol 114:2485–2499.

FitzPatrick DR, Carr IM, McLaren L, Leek JP, Wightman P, Williamson K, Gautier P, McGill N, Hayward C, Firth H, Markham AF, Fantes JA, Bonthron DT (2003) Identification of SATB2 as the cleft palate gene on 2q32–q33. Hum Mol Genet 12:2491–2501.

Fuerst PG, Bruce F, Tian M, Wei W, Elstrott J, Feller MB, Erskine L, Singer JH, Burgess RW (2009) DSCAM and DSCAML1 Function in Self-Avoidance in Multiple Cell Types in the Developing Mouse Retina. Neuron 64:484–497.

Fuerst PG, Harris BS, Johnson KR, Burgess RW (2010) A novel null allele of mouse DSCAM survives to adulthood on an inbred C3H background with reduced phenotypic variability. genesis 48:578–584.

Fuerst PG, Koizumi A, Masland RH, Burgess RW (2008) Neurite arborization and mosaic spacing in the mouse retina require DSCAM. Nature 451:470–474.

Gauthier JL, Field GD, Sher A, Greschner M, Shlens J, Litke AM, Chichilnisky EJ (2009) Receptive Fields in Primate Retina Are Coordinated to Sample Visual Space More Uniformly. PLoS Biol 7:e1000063.

Govardovskii VI, Fyhrquist N, Reuter T, Kuzmin DG, Donner K (2000) In search of the visual pigment template. Vis Neurosci 17:509–528.

Gunning DE, Chichilnisky EJ, Litke AM, O'Shea V, Smith KM, Mathieson K (2007) Performance of ultra-high-density microelectrode arrays. Nucl Instrum Methods Phys Res Sect Accel Spectrometers Detect Assoc Equip 576:215–219.

Hattar S, Liao H-W, Takao M, Berson DM, Yau K-W (2002) Melanopsin-Containing Retinal Ganglion Cells: Architecture, Projections, and Intrinsic Photosensitivity. Science 295:1065–1070.

Haverkamp S, Wässle H, Duebel J, Kuner T, Augustine GJ, Feng G, Euler T (2005) The Primordial, Blue-Cone Color System of the Mouse Retina. J Neurosci 25:5438–5445.

Hoshi H, Tian L-M, Massey SC, Mills SL (2011) Two distinct types of ON directionally selective ganglion cells in the rabbit retina. J Comp Neurol 519:2509–2521.

Huberman AD, Manu M, Koch SM, Susman MW, Lutz AB, Ullian EM, Baccus SA, Barres BA (2008) Architecture and Activity-Mediated Refinement of Axonal Projections from a Mosaic of Genetically Identified Retinal Ganglion Cells. Neuron 59:425–438.

Huberman AD, Niell CM (2011) What can mice tell us about how vision works? Trends Neurosci 34:464–473.

Huberman AD, Wei W, Elstrott J, Stafford BK, Feller MB, Barres BA (2009) Genetic Identification of an On-Off Direction- Selective Retinal Ganglion Cell

Subtype Reveals a Layer-Specific Subcortical Map of Posterior Motion. Neuron 62:327–334.

Ito S, Yeh F-C, Hiolski E, Rydygier P, Gunning DE, Hottowy P, Timme N, Litke AM, Beggs JM (2014) Large-Scale, High-Resolution Multielectrode-Array Recording Depicts Functional Network Differences of Cortical and Hippocampal Cultures. PLOS ONE 9:e105324.

Ivanova E, Hwang G-S, Pan Z-H (2010) Characterization of transgenic mouse lines expressing Cre recombinase in the retina. Neuroscience 165:233–243.

Jacobs GH, Neitz J, Deegan JF (1991) Retinal receptors in rodents maximally sensitive to ultraviolet light. Nature 353:655–656.

Jeon C-J, Strettoi E, Masland RH (1998) The Major Cell Populations of the Mouse Retina. J Neurosci 18:8936–8946.

Kandel ER, Schwartz JH, Jessell TM eds. (2000) Principles of neural science, 4th ed. New York: McGraw-Hill, Health Professions Division.

Kanjhan R, Sivyer B (2010) Two types of ON direction-selective ganglion cells in rabbit retina. Neurosci Lett 483:105–109.

Kay JN, Huerta ID la, Kim I-J, Zhang Y, Yamagata M, Chu MW, Meister M, Sanes JR (2011a) Retinal Ganglion Cells with Distinct Directional Preferences Differ in Molecular Identity, Structure, and Central Projections. J Neurosci 31:7753–7762.

Kay JN, Voinescu PE, Chu MW, Sanes JR (2011b) Neurod6 expression defines new retinal amacrine cell subtypes and regulates their fate. Nat Neurosci 14:965–972.

Kim I-J, Zhang Y, Yamagata M, Meister M, Sanes JR (2008) Molecular identification of a retinal cell type that responds to upward motion. Nature 452:478–482.

Koch C (2004) The quest for consciousness: a neurobiological approach. Denver, Colo: Roberts and Co.

Kong J-H, Fish DR, Rockhill RL, Masland RH (2005) Diversity of ganglion cells in the mouse retina: Unsupervised morphological classification and its limits. J Comp Neurol 489:293–310.

Kuffler SW (1953) Discharge Patterns and Functional Organization of Mammalian Retina. J Neurophysiol 16:37–68.

Li PH, Gauthier JL, Schiff M, Sher A, Ahn D, Field GD, Greschner M, Callaway EM, Litke AM, Chichilnisky EJ (2015) Anatomical Identification of Extracellularly Recorded Cells in Large-Scale Multielectrode Recordings. J Neurosci 35:4663–4675.

Litke AM, Bezayiff N, Chichilnisky EJ, Cunningham W, Dabrowski W, Grillo AA, Grivich M, Grybos P, Hottowy P, Kachiguine S, Kalmar RS, Mathieson K, Petrusca D, Rahman M, Sher A (2004) What does the eye tell the brain?: Development of a system for the large-scale recording of retinal output activity. IEEE Trans Nucl Sci 51:1434–1440.

London A, Benhar I, Schwartz M (2013) The retina as a window to the brain—from eye research to CNS disorders. Nat Rev Neurol 9:44–53.

Madisen L et al. (2012) A toolbox of Cre-dependent optogenetic transgenic mice for light-induced activation and silencing. Nat Neurosci 15:793–802.

Masland RH (2001) Neuronal diversity in the retina. Curr Opin Neurobiol 11:431–436.

McKendry JJD, Rae BR, Gong Z, Muir KR, Guilhabert B, Massoubre D, Gu E, Renshaw D, Dawson MD, Henderson RK (2009) Individually Addressable AlInGaN Micro-LED Arrays With CMOS Control and Subnanosecond Output Pulses. IEEE Photonics Technol Lett 21:811–813.

McKenna WL, Ortiz-Londono CF, Mathew TK, Hoang K, Katzman S, Chen B (2015) Mutual regulation between Satb2 and Fezf2 promotes subcerebral projection neuron identity in the developing cerebral cortex. Proc Natl Acad Sci 112:11702–11707.

Morin LP, Studholme KM (2014) Retinofugal projections in the mouse. J Comp Neurol 522:3733–3753.

Nagel G, Szellas T, Huhn W, Kateriya S, Adeishvili N, Berthold P, Ollig D, Hegemann P, Bamberg E (2003) Channelrhodopsin-2, a directly light-gated cation-selective membrane channel. Proc Natl Acad Sci 100:13940–13945.

Nakagomi K, Kohwi Y, Dickinson LA, Kohwi-Shigematsu T (1994) A novel DNA-binding motif in the nuclear matrix attachment DNA-binding protein SATB1. Mol Cell Biol 14:1852–1860.

Nath A, Schwartz GW (2016) Cardinal Orientation Selectivity Is Represented by Two Distinct Ganglion Cell Types in Mouse Retina. J Neurosci 36:3208–3221.

Oesch N, Euler T, Taylor WR (2005) Direction-Selective Dendritic Action Potentials in Rabbit Retina. Neuron 47:739–750.

Okawa H, Della Santina L, Schwartz GW, Rieke F, Wong ROL (2014) Interplay of Cell-Autonomous and Nonautonomous Mechanisms Tailors Synaptic Connectivity of Converging Axons In Vivo. Neuron 82:125–137.

Oyster CW, Barlow HB (1967) Direction-selective units in rabbit retina: distribution of preferred directions. Science 155:841–842.

Oyster CW, Takahashi E, Collewijn H (1972) Direction-selective retinal ganglion cells and control of optokinetic nystagmus in the rabbit. Vision Res 12:183–193.

Pang J-J, Gao F, Wu SM (2003) Light-Evoked Excitatory and Inhibitory Synaptic Inputs to ON and OFF α Ganglion Cells in the Mouse Retina. J Neurosci 23:6063–6073.

Petrusca D, Grivich MI, Sher A, Field GD, Gauthier JL, Greschner M, Shlens J, Chichilnisky EJ, Litke AM (2007) Identification and Characterization of a Y-Like Primate Retinal Ganglion Cell Type. J Neurosci 27:11019–11027.

Preibisch S, Saalfeld S, Tomancak P (2009) Globally optimal stitching of tiled 3D microscopic image acquisitions. Bioinformatics 25:1463–1465.

Provencio I, Rodriguez IR, Jiang G, Hayes WP, Moreira EF, Rollag MD (2000) A Novel Human Opsin in the Inner Retina. J Neurosci 20:600–605.

Remtulla S, Hallett PE (1985) A schematic eye for the mouse, and comparisons with the rat. Vision Res 25:21–31.

Rieke F ed. (1999) Spikes: exploring the neural code, 1. paperback ed. Cambridge, Mass.: MIT Press.

Rivlin-Etzion M, Zhou K, Wei W, Elstrott J, Nguyen PL, Barres BA, Huberman AD, Feller MB (2011) Transgenic Mice Reveal Unexpected Diversity of On-Off Direction-Selective Retinal Ganglion Cell Subtypes and Brain Structures Involved in Motion Processing. J Neurosci 31:8760–8769.

Rodieck RW (1998) The first steps in seeing. Sunderland, Mass: Sinauer Associates.

Sabbah S, Gemmer J, Castro G, Siegel J, Jeffery N, Berson DM (2015) ON-DS retinal ganglion cells encode global motion in vestibular coordinates. Invest Ophthalmol Vis Sci 56:5868–5868.

Sakai HM (1992) White-noise analysis in neurophysiology. Physiol Rev 72:491–505.

Sanes JR, Masland RH (2015) The Types of Retinal Ganglion Cells: Current Status and Implications for Neuronal Classification. Annu Rev Neurosci 38:221–246.

Savarese F, Dávila A, Nechanitzky R, Rosa-Velazquez IDL, Pereira CF, Engelke R, Takahashi K, Jenuwein T, Kohwi-Shigematsu T, Fisher AG, Grosschedl R (2009) Satb1 and Satb2 regulate embryonic stem cell differentiation and Nanog expression. Genes Dev 23:2625–2638.

Schmidt TM, Alam NM, Chen S, Kofuji P, Li W, Prusky GT, Hattar S (2014) A Role for Melanopsin in Alpha Retinal Ganglion Cells and Contrast Detection. Neuron 82:781–788.

Schmidt TM, Kofuji P (2011) An Isolated Retinal Preparation to Record Light Response from Genetically Labeled Retinal Ganglion Cells. J Vis Exp JoVE Available at: http://www.ncbi.nlm.nih.gov/pmc/articles/PMC3182668/ [Accessed February 16, 2016].

Schramm RD, Li S, Harris BS, Rounds RP, Burgess RW, Ytreberg FM, Fuerst PG (2012) A Novel Mouse Dscam Mutation Inhibits Localization and Shedding of DSCAM. PLOS ONE 7:e52652.

Sethuramanujam S, Slaughter MM (2014) Disinhibitory recruitment of NMDA receptor pathways in retina. J Neurophysiol 112:193–203.

Sher A, DeVries SH (2012) A non-canonical pathway for mammalian blue-green color vision. Nat Neurosci 15:952–953.

Shimojo S, Paradiso M, Fujita I (2001) What visual perception tells us about mind and brain. Proc Natl Acad Sci 98:12340–12341.

Sivyer B, Van Wyk M, Vaney DI, Taylor WR (2010) Synaptic inputs and timing underlying the velocity tuning of direction-selective ganglion cells in rabbit retina. J Physiol 588:3243–3253.

Srinivasan K, Leone DP, Bateson RK, Dobreva G, Kohwi Y, Kohwi-Shigematsu T, Grosschedl R, McConnell SK (2012) A network of genetic repression and derepression specifies projection fates in the developing neocortex. Proc Natl Acad Sci 109:19071–19078.

Sümbül U, Song S, McCulloch K, Becker M, Lin B, Sanes JR, Masland RH, Seung HS (2014) A genetic and computational approach to structurally classify neuronal types. Nat Commun 5:3512.

Sun W, Li N, He S (2002) Large-scale morphological survey of mouse retinal ganglion cells. J Comp Neurol 451:115–126.

Tang JCY, Rudolph S, Dhande OS, Abraira VE, Choi S, Lapan SW, Drew IR, Drokhlyansky E, Huberman AD, Regehr WG, Cepko CL (2015) Cell type-specific manipulation with GFP-dependent Cre recombinase. Nat Neurosci 18:1334–1341.

Thoreson WB, Babai N, Bartoletti TM (2008) Feedback from Horizontal Cells to Rod Photoreceptors in Vertebrate Retina. J Neurosci 28:5691–5695.

Trenholm S, Johnson K, Li X, Smith RG, Awatramani GB (2011) Parallel Mechanisms Encode Direction in the Retina. Neuron 71:683–694.

Van Wyk M, Wässle H, Taylor WR (2009) Receptive field properties of ON- and OFF-ganglion cells in the mouse retina. Vis Neurosci 26:297–308.

Völgyi B, Chheda S, Bloomfield SA (2009) Tracer coupling patterns of the ganglion cell subtypes in the mouse retina. J Comp Neurol 512:664–687.

Wang YV, Weick M, Demb JB (2011) Spectral and Temporal Sensitivity of Cone-Mediated Responses in Mouse Retinal Ganglion Cells. J Neurosci 31:7670–7681.

Wässle H (2004) Parallel processing in the mammalian retina. Nat Rev Neurosci 5:747–757.

Wassle H, Boycott BB (1991) Functional architecture of the mammalian retina. Physiol Rev 71:447–480.

Wassle H, Boycott BB, Illing R-B (1981) Morphology and Mosaic of on- and off-Beta Cells in the Cat Retina and Some Functional Considerations. Proc R Soc Lond B Biol Sci 212:177–195.

Wei W, Elstrott J, Feller MB (2010) Two-photon targeted recording of GFP-expressing neurons for light responses and live-cell imaging in the mouse retina. Nat Protoc 5:1347–1352.

Wei W, Feller MB (2011) Organization and development of direction-selective circuits in the retina. Trends Neurosci 34:638–645.

Weng S, Sun W, He S (2005) Identification of ON–OFF direction-selective ganglion cells in the mouse retina. J Physiol 562:915–923.

Xiang M, Zhou L, Macke JP, Yoshioka T, Hendry SH, Eddy RL, Shows TB, Nathans J (1995) The Brn-3 family of POU-domain factors: primary structure, binding

specificity, and expression in subsets of retinal ganglion cells and somatosensory neurons. J Neurosci 15:4762–4785.

Yonehara K, Ishikane H, Sakuta H, Shintani T, Nakamura-Yonehara K, Kamiji NL, Usui S, Noda M (2009) Identification of Retinal Ganglion Cells and Their Projections Involved in Central Transmission of Information about Upward and Downward Image Motion. PLoS ONE 4:e4320.

Zhang F, Wang L-P, Boyden ES, Deisseroth K (2006) Channelrhodopsin-2 and optical control of excitable cells. Nat Methods 3:785–792.

Zhang Y, Kim I-J, Sanes JR, Meister M (2012) The most numerous ganglion cell type of the mouse retina is a selective feature detector. Proc Natl Acad Sci Available at: http://www.pnas.org/content/early/2012/08/08/1211547109 [Accessed March 15, 2013].

Zhao X, Chen H, Liu X, Cang J (2013) Orientation-selective Responses in the Mouse Lateral Geniculate Nucleus. J Neurosci 33:12751–12763.

Zhao X, Stafford BK, Godin AL, King WM, Wong KY (2014) Photoresponse diversity among the five types of intrinsically photosensitive retinal ganglion cells. J Physiol 592:1619–1636.

Zhu Y, Xu J, Hauswirth WW, DeVries SH (2014) Genetically Targeted Binary Labeling of Retinal Neurons. J Neurosci 34:7845–7861.